Electronic structure of icosahedral $Al_{65}Cu_{20}Ru_{15}$ studied by photoemission spectroscopy

Z. M. Stadnik* and G. W. Zhang
Department of Physics, University of Ottawa, Ottawa, Ontario, Canada K1N 6N5

A.-P. Tsai and A. Inoue
Institute for Materials Research, Tohoku University, Sendai 980, Japan
(Received 5 July 1994)

Measurements with photoemission spectroscopy in the photon-energy range 40–140 eV have been used to determine the valence band of the stable icosahedral $Al_{65}Cu_{20}Ru_{15}$. Resonant photoemission near the Ru $4p \rightarrow 4d$ transition has been employed to show that the feature in the valence band with the maximum intensity at 1.3(1) eV below the Fermi level is predominantly of Ru $4d$ character. This has been additionally verified by conducting the photoemission measurements in the constant-initial-state mode and by using the effect of the Cooper minimum in the photoionization cross section of the Ru $4d$ orbitals. The valence-band feature with the maximum intensity at 3.8(1) eV below the Fermi level has been shown as being due mainly to the states of Cu $3d$ character. The Ru $4d$ and Cu $3d$ empirical partial density of states have been determined from the photoemission spectra. The decrease of intensity towards the Fermi level has been interpreted as being indicative of the presence of a theoretically predicted pseudogap around the Fermi level. It has been indicated, however, that the Fermi cutoff also contributes to the observed intensity decrease. It has been demonstrated that the energy resolution of the spectroscopic measurements performed so far on quasicrystals was not high enough to unambiguously determine the presence of such a pseudogap. No unusual features in the valence band of icosahedral $Al_{65}Cu_{20}Ru_{15}$, which could be ascribed to its quasiperiodic nature, have been observed within the resolution of the experiment. The need of high-energy-resolution spectroscopic measurements, which are essential in order to observe the theoretically predicted spikiness of the density of states in quasicrystals, has been emphasized. A review of published experimental data on the electronic structure of quasicrystals has also been presented.

I. INTRODUCTION

Solids are traditionally grouped into two categories: crystalline and amorphous. The discovery of an icosahedral Al-Mn alloy by Shechtman *et al.*[1] extended this dichotomous division by introducing the notion of quasicrystals (QC's). This form of matter has an unusual type of long-range translational order, which is called *quasiperiodicity,* and noncrystallographic orientational order associated with the fivefold, eightfold, tenfold, and twelvefold symmetry axes.[2,3] A central problem in condensed-matter physics is to determine whether quasiperiodicity leads to physical properties which are significantly different from those of crystalline and amorphous materials.

In the first few years following the discovery of QC's, their experimental physical properties were found to be similar to either their corresponding crystalline or amorphous counterparts.[4–7] It was later realized that the first QC's, which were thermodynamically *metastable,* possessed significant structural disorder, as manifested in the broadening of the x-ray-diffraction lines, and contained some amount of second phases. It was argued that this prevented detecting possible physical properties intrinsic to quasiperiodicity. Opportunities for experimental studies of QC's have emerged when the first thermodynamically *stable* icosahedral (*i*) alloys Al-Cu-(Fe, Ru, Os) (Ref. 8) and Al-Pd-(Mn, Re) (Ref. 9) were discovered because they possess a high degree of structural perfection comparable to that found in the best periodic alloys. Indeed these *i*-alloys exhibit some unusual behavior. Their most characteristic features, which are not expected for alloys formed of normal metallic elements, are the very high value of the electrical resistivity [up to 0.01 Ω cm in Al-Cu-Fe and Al-Pd-Mn alloys at 4.2 K,[7,10] up to 0.03 Ω cm in Al-Cu-Ru alloys,[7] and up to the record high value of 0.28 Ω cm in Al-Pd-Re alloys;[11,12] the resistivity of the *i*-$Al_{70}Pd_{20}Re_{10}$ alloy reaches about 1 Ω cm at 0.45 K (Ref. 11)], and its temperature coefficient which is generally negative. This puts them at the border of the metal-insulator transition. It was even suggested[11] that *i*-Al-Pd-Re alloys are in fact quasiperiodic insulators. The resistivity of these *i* alloys depends on the structural quality of the sample used in an unexpected way; it increases when the structural defects are removed,[12] in contrast to the behavior of typical metals. Additionally, the resistivity is extremely sensitive to sample composition,[12,13] which is reminiscent of doping effects in semiconductors. Other anomalies in transport properties of QC's, such as low electronic contribution to the specific heat, large and strongly temperature-dependent Hall coefficients and thermoelectric power, or a non-Drude-like optical conductivity, have been also observed and are reviewed in Refs. 7 and 14.

Magnetic properties of metastable Al-Mn-based *i* alloys, which are reviewed in Ref. 15, do not exhibit any

unusual behavior. These alloys are typical paramagnets and some of them show a spin-glass behavior at low temperatures. As was argued in Ref. 15, these properties result from the disorder present in these metastable alloys rather than from intrinsic properties induced by icosahedral symmetry. The first indication of the unusual magnetic behavior of stable *i* alloys came from the low-temperature magnetic susceptibility measurements,[15] which showed that *i*-$Al_{65}Cu_{20}Fe_{15}$ alloy is a diamagnet between 1.5 and 77 K, in spite of a significant concentration of Fe in the alloy. Diamagnetism was shown also to exist between 77 and 650 K,[16] and was confirmed later in other studies of the *i*-Al-Cu-Fe system.[13,17,18] Diamagnetism was also observed in the *i*-Al-Pd-Mn alloy.[19] It is worth noticing that samples corresponding to the compositions of the stable *i* alloys, but containing some degree of disorder or small amounts of parasitic phases, generally exhibit a paramagnetic behavior.[20] It thus seems that a physical measure of a high quality of an *i* alloy, which at the same time reflects its intrinsic property, is the high resistivity and diamagnetism.[19]

Results on the electronic transport measurements on QC's have been interpreted almost exclusively in terms of a "Hume-Rothery" effect, which has been attributed a range of validity far beyond that suggested by the free-electron form of the original argument. The anomalously low electrical conductivity (high resistivity) and the low electronic specific-heat coefficient were taken as evidence for the existence of a pseudogap in the density of states (DOS) at the Fermi level E_F.[7,14] This pseudogap, in turn, is believed to result from the Hume-Rothery mechanism of the stability of QC's, which implies an interaction of the pseudo-Brillouin zone with the Fermi surface. Thus, the Hume-Rothery mechanism can be used to explain why the stable QC's have the lowest conductivity, the lowest electronic specific-heat coefficient, and can exist in a rather narrow compositional range (too large a composition change shifts E_F from a pseudogap to higher DOS). The existence of a pseudogap at E_F is also predicted by theory based on the nearly-free-electron approximation[21] and by the electronic structure calculations for the lowest-order crystalline approximants.[22–25] It is worth noting that theoretical calculations by Hafner and Krajčí[24] suggest that, although the structure-induced pseudogap at the Fermi level is a *generic* property of QC's, it is not a *specific* property distinguishing the quasiperiodic from the periodic or aperiodic phases because it is also present in some amorphous and crystalline alloys.[24] This seems to be in accord with the recent NMR results[26] which show low values of DOS (E_F) in both *i* alloys and their crystalline approximants.

There is another mechanism[27] which claims to give a good explanation of electronic transport properties of QC's and which avoids some problems[27] associated with extending the Hume-Rothery argument to alloys with *d* elements. It is based on an internal structural model which assumes the presence of the conductive *i* blocks which are enveloped by an insulating layered-structure network. For this structural model the electrical conduction occurs via tunneling.[27] Other mechanisms invoked to explain the electronic-transport properties of QC's are based on intraband transitions via electron hopping descriptions[28] or on the criticality of the wave functions.[29] It can be concluded that at present there seems to be no generally accepted explanation for the unusual electronic-transport properties of QC's.

The electrical conductivity of stable *i* alloys in the low-temperature range has a characteristic temperature dependence: it is proportional to $\sqrt{T}$ for the lowest temperatures and to T at higher temperatures.[7,14,30] These temperature dependencies, as well as those of magnetoresistance, are explained using quantum interference theories (the electron-electron interaction and weak-localization effects).[7,14,30] However, such theories were originally developed for highly disordered conductors. Thus, their apparent relevance to stable *i* alloys suggests that these alloys are electronically disordered. This, however, poses a question: how can such electronic disorder be reconciled with the apparent high degree of local atomic order in stable *i* alloys, as determined by diffraction and electron-microscopy experiments? We suggest one plausible explanation of this apparent contradiction. There are at present 22 known stable QC's: 14 *i*-systems Al-Cu-Li, Mg-Ga-Zn, Al-Cu-(Fe, Ru, Os), Al-Pd-(Mn,Re), and the recently discovered Al-Pd-Mg (Ref. 31) and Zn-Mg-RE (RE=Y, Gd, Tb, Dy, Ho, Er),[32] and eight decagonal systems Al-Co-(Cu, Ni), Al-Pd-Mn, Al-Rh-(Cu, Ni), and Al-Pd-(Fe, Ru, Os). They are all ternary alloys and 15 of them are based on aluminum. If one envisages that their structure consists of an *sp*-type sublattice and a *d*-type sublattice, then clearly one expects the presence of chemical disorder in these sublattices (for example, in the CuFe, CuRu, CuOs, PdMn, PdRe sublattice). Furthermore, the concept of quasiperiodicity implies that no two crystallographic positions of a given atom are exactly the same,[33] which can be viewed as a sort of topological disorder. Although these two types of disorder are not seen in the diffraction and electron microscopy experiments on stable QC's, they are clearly detected, but not separated, in other experiments which are more sensitive to the presence of such disorder. For example, local probes such as Mössbauer spectroscopy,[15] (NMR),[34] or nuclear quadrupole resonance (NQR),[35] clearly detect the presence of a distribution of quadrupole splittings in high-quality stable *i* alloys. Such a distribution can be detected only if there is a chemical and/or topological disorder in the investigated samples. Also the NMR parameters, the Knight shift, and the spin-lattice relaxation rate, indicate the presence of some disorder modes.[34] A recent study on the propagation of acoustic shear waves in a single-grain *i*-Al-Pd-Mn alloy shows the similarity of the acoustic properties of this alloy to those of amorphous metals.[36] These experiments[15,34–36] demonstrate that chemical and/or topological disorder is present also in the high-quality phason-free stable *i* alloys and it must be taken into account in attempts to understand the physical properties of QC's. In particular, chemical disorder may be responsible for the success of quantum interference theories mentioned above (topological disorder produced by quasiperiodicity cannot be directly associated with these theories because they start with Bloch waves and perturb them with disor-

der, whereas wave functions in QC's cannot be written as perturbed Bloch states).

Electronic transport measurements discussed above made a significant contribution to our understanding of the electronic structure of QC's. It should be remembered, however, that these measurements provide *indirectly* information on the DOS at one particular energy (E_F). To determine the electronic structure of QC's one needs information not only on the DOS (E_F), but also on the DOS below and above E_F. Therefore, studies using spectroscopic techniques which probe DOS *directly* at energies in the vicinity of E_F are extremely useful. The x-ray-photoelectron spectroscopy (XPS), photoemission spectroscopy (PES), and soft-x-ray-emission (SXE) spectroscopy were employed to study the DOS below E_F, whereas the DOS above E_F was probed with the inverse photoemission spectroscopy (IPES) and soft-x-ray-absorption (SXA) spectroscopy in Al-Mn-Si, Al-Li-Cu-Mg, Al-Cu-Fe-Cr, Al-Pd-Mn, Al-Ga-Mg-Zn, and Al-Cu-Mn QC's.[4,5,37–51] These electronic structure studies lead to several conclusions, which will be discussed in detail in Sec. III in relation to the present study, and which are summarized below. First, the most important finding is the apparent observation of the pseudogap at E_F, which is predicted by theory and suggested by the results of electronic transport measurements, in some of the studied QC's. However, an unambiguous spectroscopic verification of the existence of such a psuedogap for QC's containing the transition-metal (TM) elements is very difficult because the experimentally measured intensity in the vicinity of E_F is dominated by the TM 3*d* states, as is well known from similar studies of the structurally induced minimum in the DOS in amorphous alloys.[52] Second, chemical shifts of the Al 2*p* lines are either zero or very small with respect to similar crystalline compounds or pure elements. This is at odds with the theoretical result[53] which predicts large shifts (0.8 eV), and thus confirms the conclusion of recent theoretical studies[54] of the unreliability of the theoretical predictions[53] based on calculations performed on small clusters. Third, a close structural similarity between the valence-band spectra of QC's and those of the corresponding crystalline compounds was found. No dense and sharp features in the DOS of QC's predicted by the theory[21–25] were observed. Finally, various measured spectral features were ascribed to particular electronic states of *s*, *p*, and *d* character, and evidence of hybridization between *sp* and *d* states was presented.

The majority of physical measurements have been performed so far on stable Al-Cu-Fe (Refs. 2, 3, 7, 10, 13–15, 26, 28, 34, 35, 39, and 43–49) and Al-Pd-Mn (Refs. 10, 14, 28, 30, 36, 45, 47, and 51) *i* alloys. Fewer studies were conducted on *i*-Al-Cu-Ru and Al-Cu-Os alloys. Most of the studies carried out on *i*-Al-Cu-Ru alloys are associated with their various structural aspects and were done using x-ray-diffraction XRD) (Refs. 55–61), extended x-ray-absorption fine-structure,[62] and electron-diffraction and electron-microscopy techniques.[56,57,61,63] These structural studies established that the *i*-Al-Cu-Ru alloys are similar to *i*-Al-Cu-Fe and Al-Pd-Mn alloys in that they are face-centered icosahedral (FCI) alloys with an enhanced degree of chemical and topological order as manifested in the disappearance of phason disorder. In contrast to the situation for *i*-Al-Cu-Fe (Ref. 64) or Al-Pd-Mn,[65] no six-dimensional structural analysis has been done for the *i*-Al-Cu-Ru alloys yet.

The electrical resistivity of *i*-Al-Cu-Ru alloys strongly increases with decreasing temperature.[66–71] The electrical conductivity of the *i*-Al-Cu-Ru alloys[66,69,71] is close to the minimum metallic conductivity of about 200 $\Omega^{-1}\,cm^{-1}$,[72] and thus these alloys can be regarded as semimetals. The specific heat measurements[66,67,69] give the value of the linear electronic coefficient γ which, for a high-quality sample, is only about 10% of the estimated free-electron value. This suggests a very low DOS (E_F) and was taken, together with a strong variation of γ with composition, as evidence[66,67,69] of the presence of a structure-induced minimum of the density of states at the Fermi level. On the basis of the observed temperature dependence of the Hall coefficient and thermopower, it was suggested that rapidly varying structures may exist in the DOS of *i*-Al-Cu-Ru alloys.[66,69]

The first ^{27}Al and ^{63}Cu NMR experiment on *i*-$Al_{65}Cu_{20}Ru_{15}$ concluded from the temperature independence of the Knight shift between 5 K and room temperature[73] that this alloy is a Pauli paramagnet. This conclusion about the temperature independence of the Knight shift was confirmed in the next NMR study.[34] This study found[34] that the composition independence of the NMR parameters which are proportional to the DOS (E_F) is difficult to reconcile with the γ dependence on composition;[66,69] the possibility of the presence of the disorder modes in the stable *i*-Al-Cu-Ru was suggested. A recent NMR study of *i*-$Al_{65}Cu_{20}Ru_{15}$[74] found the unusual temperature dependence of the Knight shift above 500 K, which was interpreted in terms of the presence of a pseudogap at the Fermi level. The first ^{27}Al NQR study of *i*-$Al_{70}Cu_{15}Ru_{15}$ found[35] a continuous distribution of the NQR signal which was attributed to a multiplicity of nonequivalent Al sites.

This paper reports the first thorough study of the electronic structure of a high-quality *i*-$Al_{65}Cu_{20}Ru_{15}$ alloy using the synchrotron-radiation-based PES technique. By employing the photon-energy dependence of the photoionization cross section and the effect of a core-electron resonance, we are able not only to identify the origin of the prominent features in the valence band of the studied alloy, but also to separate the overlapping contributions due to the Cu 3*d* and Ru 4*d* states. Before the emergence of the synchrotron-radiation-based PES technique, such a separation of contributions of a given symmetry (*s*, *p*, *d*, or *f*) due to a specific element could be only obtained from the SXE techniques. A critical review of the published spectroscopic evidence for the existence of a pseudogap at the Fermi energy in stable QC's is also presented.

II. EXPERIMENTAL PROCEDURE

An alloy of composition $Al_{65}Cu_{20}Ru_{15}$ was produced by arc melting high-purity elemental constituents in ar-

gon. It was annealed between 1123 and 1173 K for 48 h in vacuum, and then cut into slices suitable for PES measurements. The details of the sample preparation are described elsewhere.[8]

XRD measurements on powder obtained from the slices of the $Al_{65}Cu_{20}Ru_{15}$ alloy chosen for PES studies were performed on a Philips X'Pert scanning diffractometer equipped with a PW3020 vertical goniometer with a 173-mm radius and with a long fine focus Cu-target tube operated at 45 kV and 40 mA. This goniometer uses dc motors instead of conventional stepper motors and the Θ and 2Θ angles are monitored via two optical encoder disks mounted directly on a drive shaft. This allows the 2Θ accuracy of about 0.003° to be achieved. The data were recorded by automatic step scanning with a step width of 0.02° 2Θ. To allow for the possible instrumental aberration and specimen displacement, corrections were made to the 2Θ angles using a fourth-order polynomial calibration curve[75] obtained from the scan of the specimen mixed with 10 wt. % of a Si standard (National Bureau of Standards reference material 640b). The diffractometer was equipped with a variable divergence slit which kept the illuminated length of the sample constant at 12.5 mm, and a 0.1 mm receiving slit was used. With this setting the instrumental resolution, as determined from the full width at half maximum of the (111) peak of a Si standard, was 0.007 Å^{-1}. A fine sample powder was mixed with methanol and allowed to dry on a low-background sample holder cut from a single crystal of Si, resulting in a thin flat sample. A sample spinner was used to further minimize a possible preferred sample orientation. Cu $K\alpha$ radiation was employed and the $K\beta$ line was eliminated by using a Kevex PSi2 Peltier cooled Si detector. In order to avoid the deviation from linearity of the detector used, its parameters and the parameters of the diffractometer were chosen in such a way as to limit the count rate from the most intense peak to less than 9000 Hz.[76]

Photoemission spectra were collected on beamline U14A at the National Synchrotron Light Source at Brookhaven National Laboratory. Photon energies between 40 and 140 eV were selected with a plane grating monochromator. The normal to the sample was at an angle of 45° to both the photon beam and the axis of a PHI 15-255 precision electron energy analyzer. The resulting overall resolution was 0.4 eV. The sample was cleaned in the experimental vacuum chamber either by 1.5-keV Ar^+ bombardment for a few minutes or by gentle mechanical abrasion using an alumina scraper. No differences between the PES spectra corresponding to these two surface-treatment methods could be detected. The surface cleanliness of the sample was frequently checked by monitoring the appearance of the oxide features in the Al $2p$ line and/or in the valence band.[48] The base pressure in the experimental chamber was in the high 10^{-11}-Torr range. No effects due to a possible charge build up were observed during the PES experiments.

All the spectra presented in this work were obtained from at least two different regions of the sample studied, and turned out to be indistinguishable within the resolution of the experiment. The position of the Fermi level was determined with an accuracy of 0.05 eV by measuring the Fermi edge and/or the Al $2p$ line (for photon energies larger than 100 eV) of an adjacent Al sample. It was additionally verified by a linear extrapolation of the leading edge of the valence band of the measured spectra.

III. RESULTS AND DISCUSSION

A. X-ray-diffraction data

The XRD spectrum of the studied sample measured in the 2Θ range 7–128° (Fig. 1) shows the presence of many Bragg lines, the weaker of which are usually not observed in the spectra obtained with a scintillation or a proportional counter. This increased sensitivity for weak lines is due to the solid-state detector which has a higher counting efficiency (due to the elimination of a monochromator in the diffracted beam) and lower-background count rate as compared to more conventional detectors used in combination with a diffracted-beam monochromator. The positions of all the detected Bragg lines corresponding to Cu $K\alpha_1$ radiation [the value of its wavelength λ currently accepted by the National Institute for Standards and Technology is 1.540 598 1 Å (Ref. 77)] in terms of the angle $2\Theta_1$ and the corresponding wave number $Q_{\text{expt}}=4\pi\sin\Theta_1/\lambda$, as well as their relative intensities and full widths at half maximum Γ_Q, were determined from the profile fitting using the procedure described by Schreiner and Jenkins.[78] These parameters corresponding to 47 detected i peaks, whose positions are indicated by the vertical lines in Fig. 1, are presented in Table I together with the calculated (taking the line number 16 as the reference line) line positions Q_{cal} and the corresponding indexes. Since there are several schemes employed to index the i lines, we present the indexes corresponding to the most commonly used schemes[79–81] in order to enable the reader to make convenient identification of the i lines.

Most of the observed Bragg lines can be indexed to the i structure. It is noticeable that even the peaks with an intensity as small as 0.1% of the most intense peak could be detected and indexed to the i structure (Fig. 1 and Table I). There is an excellent agreement between the observed Q_{expt} and theoretical Q_{cal} positions (Table I) of the peaks. Out of 47 detected i peaks, 42 are at the positions within ± 0.001 Å^{-1} and only five (peaks number 32, 38, 42, 44, and 45) within ± 0.002 Å^{-1} of the values calculated for the six-dimensional FCI lattice. The widths of most i peaks (Table I) are found to be limited by the instrumental resolution. The presence of the superlattice lines (Fig. 1 and Table I), for which N in the N/M index[79] is equal to $4n+3$ (the strongest superlattice line is the line number 6),[82] confirms[55,57] that i-$Al_{65}Cu_{20}Ru_{15}$ has the six-dimensional direct FCI cubic Bravais lattice. The value of the six-dimensional cubic lattice constant $a_{6D}=6.402$ Å is in a good agreement with values found in the literature.[55,56] An analysis similar to that performed by Guryan *et al.*[55] for the Bragg peaks with the intensity (INT) values larger than 2% (Table I) shows a linear dependence of Γ_Q on the measured momentum transfer Q_{expt} and no systematic dependence on the

phason momentum $Q_\perp$. This shows that the studied alloy has no phason disorder.

All other weak nonicosahedral Bragg peaks in Fig. 1 could be identified with the peaks due to the presence of a very small amount of the orthorhombic Al_2Ru (Joint Committee on Powder Diffraction Standards file 19-0045) and tetragonal Al_2Cu (JCPDS file 25-0012) alloys as the second phases. Such weak peaks usually are not detected with a conventional proportional or scintillation counter. It is thus concluded that the studied sample is predominantly single-phase phasonless *i* alloy.

B. Methodology of evaluation of the raw photoemission spectra

In order to compare the intensities of the synchrotron-radiation-based PES spectra of a given sample, several corrections have to be taken into account. All our PES spectra presented here were correlated first for the energy dependence of the electron transmission of the electron energy analyzer. It was assumed that the transmission of the analyzer, including the retarding lens system, is inversely proportional to the kinetic energy of the electrons, as has been shown by Helmer and Weichert.[83] Next, the PES spectra were normalized for the time-dependent photon flux, and the secondary-electron contribution was subtracted by assuming that secondary-electron background intensity at each binding energy (E_B) is proportional to the total integrated signal at lower binding energies.[84] The first two corrections slightly change the shape of the original spectrum, whereas the third one produces the largest changes (Fig. 2). It can be also seen (Fig. 2) that the corrections have no significant influence on the shape of the spectrum close to E_F, but change the spectrum substantially at higher binding energies (the negative value of E_B in Fig. 2 indicates the energy scale below E_F). The PES spectra corrected in such a way can be compared not only with respect to their shape but also in terms of their intensities. This is especially

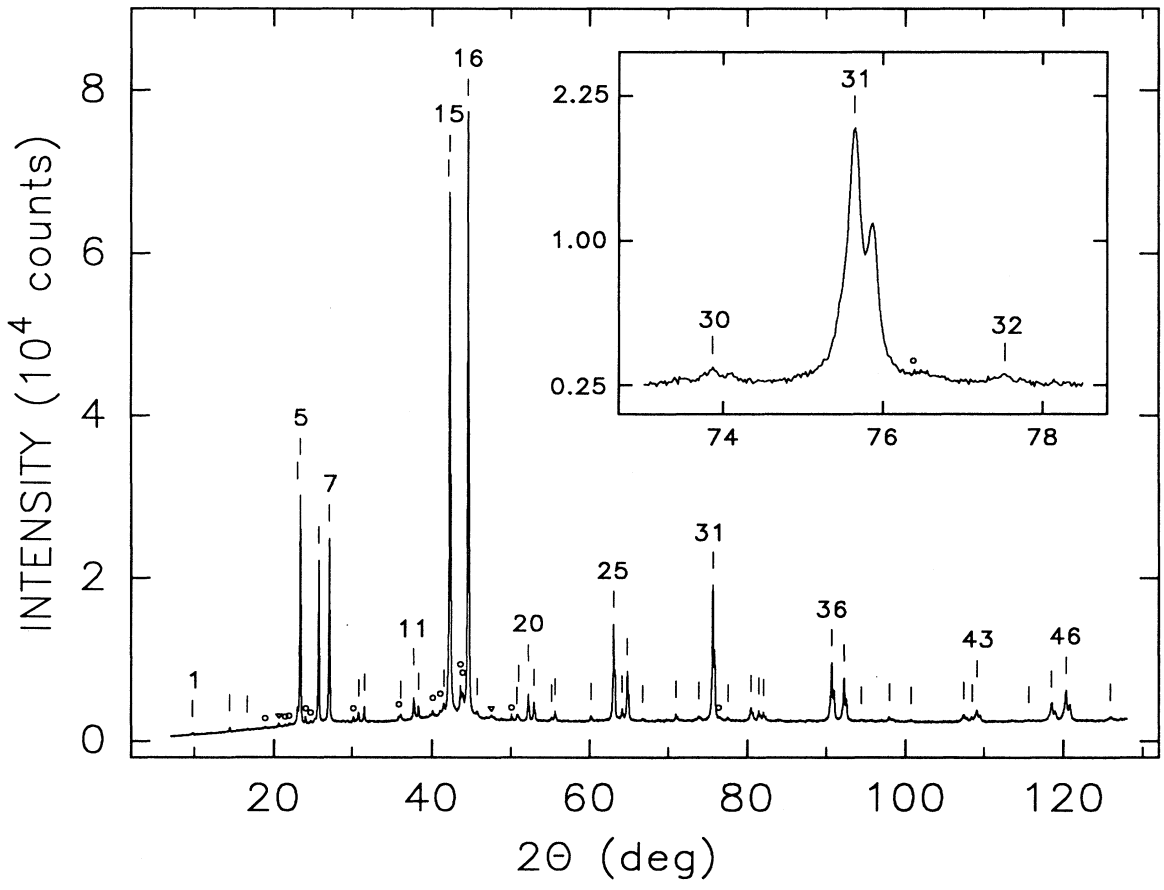

FIG. 1. X-ray-diffraction spectrum of an $Al_{65}Cu_{20}Ru_{15}$ alloy. For clarity, only some of the detected *i* peaks are labeled with integers and the vertical lines above all detected *i* peaks correspond to the positions calculated for the Cu $K\alpha_1$ radiation, as described in the text. Notice the splitting of diffraction peaks for larger 2Θ values due to $K\alpha_2$ radiation. The position, full width at half maximum, and relative intensity of each detected *i* peak determined from the fit (Ref. 78) are given in Table I together with the corresponding index. The symbols (○) and (▽) indicate the peak positions corresponding, respectively, to the strongest peaks of the orthorhombic Al_2Ru and tetragonal Al_2Cu second phases. The inset shows a part of the spectrum with low-intensity peaks. Note the square-root scale on the ordinate axis of the inset, which makes low-intensity peaks more visible.

TABLE I. The position in terms of $2\Theta_1$ (in degrees) corresponding to Cu $K\alpha_1$ radiation and Q_{expt} (in Å^{-1}), the full width at half maximum Γ_Q (in Å^{-1}), and the relative intensity INT normalized to 100.0 of all detected i peaks, which are labeled with consecutive integers in column 1, as obtained from the fit (Ref. 78). The integers in the first column correspond to the vertical lines in Fig. 1. Q_{cal} (in Å^{-1}) is the calculated Q value by taking the line number 16 as the reference line. $I1$ and $I2$ are the indexes (N/M) and $(h/h',k/k',l/l')$ based on the indexing scheme of Cahn, Shechtman, and Gratias (Ref. 79), whereas $I3$ and $I4$ are the indexes corresponding, respectively, to the indexing schemes of Elser (Ref. 80) and Bancel *et al.* (Ref. 81). The symbol $n_1n_2n_3n_4n_5n_6/2$ in the $I3$ and $I4$ schemes is an abbreviation for the index $\frac{n_1}{2}\frac{n_2}{2}\frac{n_3}{2}\frac{n_4}{2}\frac{n_5}{2}\frac{n_6}{2}$. The FCI superlattice lines are those for which $N=4n+3$ in the $I1$ scheme and which have the indexes in the form $n_1n_2n_3n_4n_5n_6/2$ in the $I3$ and $I4$ schemes.

Label	$2\Theta_1$	Q_{expt}	Q_{cal}	Γ_Q	INT	$I1$	$I2$	$I3$	$I4$
1	9.760	0.694	0.694	0.010	0.2	2/1	011 000	100 000	$21\bar{1}\,\bar{1}\,\bar{1}1$
2	14.410	1.023	1.022	0.009	0.4	3/3	101 100	$111\,11\bar{1}/2$	$331\,\bar{1}\,\bar{3}1/2$
3	16.630	1.180	1.181	0.011	0.1	4/4	000 200	110 000	$220\,0\bar{1}1$
4	23.049	1.630	1.629	0.015	1.6	7/8	112 100	$311\,11\bar{1}/2$	$53\bar{1}\,\bar{1}\,\bar{3}3/2$
5	23.385	1.653	1.654	0.009	30.2	6/9	011 200	111 000	110 001
6	25.735	1.816	1.817	0.008	22.4	7/11	111 200	$311\,111/2$	$111\,1\bar{1}1/2$
7	27.088	1.910	1.910	0.009	26.1	8/12	002 200	111 100	$111\,0\bar{1}0$
8	30.794	2.166	2.167	0.011	1.3	11/15	101 300	$331\,1\bar{1}1/2$	$53\bar{1}\,\bar{1}\,\bar{1}3/2$
9	31.521	2.216	2.216	0.009	2.1	11/16	011 300	$331\,111/2$	$331\,1\bar{1}3/2$
10	36.100	2.527	2.527	0.011	0.9	14/21	102 300	211 100	$210\,0\bar{1}1$
11	37.724	2.637	2.636	0.012	3.0	15/23	121 300	$333\,111/2$	$331\,1\bar{1}1/2$
12	38.312	2.677	2.677	0.010	1.8	15/24	112 300	$333\,1\bar{1}1/2$	$111\,111/2$
13	41.479	2.889	2.889	0.005	1.0	19/27	103 300	$531\,111/2$	$551\,\bar{1}\,\bar{3}1/2$
14	42.054	2.927	2.926	0.009	5.5	19/28	013 300	$333\,311/2$	$531\,\bar{1}\,\bar{3}1/2$
15	42.249	2.940	2.940	0.009	85.9	18/29	122 300	211 111	100 000
16	44.535	3.091	3.091	0.010	100.0	20/32	002 400	221 001	110 000
17	45.696	3.167	3.168	0.017	0.4	22/33	012 410	221 101	$221\,0\bar{1}1$
18	50.737	3.495	3.494	0.008	0.5	27/40	103 410	$533\,31\bar{1}/2$	$551\,1\bar{1}3/2$
19	50.922	3.506	3.506	0.014	0.4	26/41	013 400	222 100	111 101
20	52.157	3.586	3.585	0.010	4.6	27/43	113 400	$533\,311/2$	$311\,\bar{1}\,\bar{1}1/2$
21	52.916	3.634	3.634	0.010	3.1	28/44	222 400	311 111	210 001
22	55.143	3.775	3.775	0.013	0.5	31/47	132 410	$553\,111/2$	$531\,\bar{1}\,\bar{3}3/2$
23	55.596	3.804	3.803	0.012	1.5	31/48	112 500	$553\,1\bar{1}1/2$	$53\bar{1}\,\bar{1}\,\bar{1}1/2$
24	60.181	4.090	4.089	0.013	0.8	35/56	013 500	$553\,113/2$	$311\,1\bar{1}1/2$
25	63.068	4.266	4.266	0.011	16.3	38/61	233 400	$322\,101$	111 000
26	64.160	4.332	4.331	0.008	1.6	39/63	123 500	$555\,1\bar{1}1/2$	$111\,11\bar{1}/2$
27	64.821	4.372	4.371	0.010	8.8	40/64	242 400	$322\,111$	111 100
28	66.762	4.488	4.489	0.015	0.4	43/67	333 400	$733\,331/2$	$531\,1\bar{1}3/2$
29	70.972	4.735	4.734	0.011	1.1	47/75	113 600	$753\,113/2$	$331\,\bar{1}\,\bar{1}\,\bar{1}/2$
30	73.872	4.902	4.901	0.008	0.8	51/80	134 500	$755\,1\bar{1}1/2$	$531\,\bar{1}\,\bar{1}\,3/2$
31	75.650	5.002	5.001	0.011	24.5	52/84	004 600	$332\,002$	101 000
32	77.528	5.107	5.105	0.008	0.5	55/87	133 600	$755\,3\bar{1}1/2$	$531\,\bar{1}\,\bar{1}1/2$
33	80.482	5.269	5.268	0.013	2.3	58/93	233 600	$333\,101$	210 000
34	81.454	5.322	5.321	0.010	1.7	59/95	343 500	$755\,313/2$	$311\,111/2$
35	82.066	5.355	5.354	0.010	1.4	60/96	224 600	$422\,211$	$210\,\bar{1}00$
36	90.688	5.802	5.801	0.012	10.0	70/113	124 700	$432\,112$	110 010
37	92.263	5.880	5.879	0.011	7.9	72/116	244 600	$433\,101$	200 000
38	94.447	5.987	5.985	0.009	0.3	75/120	015 700	$955\,313/2$	$511\,\bar{1}\,\bar{1}1/2$
39	97.978	6.155	6.154	0.006	0.8	79/127	125 700	$955\,333/2$	$331\,\bar{1}\,\bar{1}1/2$
40	100.772	6.284	6.283	0.010	0.4	83/132	334 700	$975\,113/2$	$531\,113/2$
41	107.400	6.574	6.573	0.013	1.3	90/145	015 800	$522\,222$	111 110
42	108.448	6.618	6.616	0.013	0.7	91/147	115 800	$975\,115/2$	$311\,\bar{1}1\bar{1}/2$
43	109.070	6.643	6.642	0.012	2.1	92/148	115 801	$443\,102$	211 000
44	115.652	6.904	6.902	0.002	0.1	99/160	354 700	$977\,313/2$	$311\,11\bar{1}/2$
45	118.490	7.010	7.008	0.011	3.2	102/165	235 800	$444\,1\bar{1}1$	101 010
46	120.293	7.074	7.073	0.014	5.5	104/168	464 600	$533\,212$	111 010
47	125.887	7.264	7.264	0.012	0.5	110/177	364 700	$543\,102$	211 100

important when the intensity scale of the PES spectra is used, as is the case in this paper, to obtain information on various features of the valence bands and on the partial DOS due to a specific element in an alloy.

C. Structure of the valence band

The structure of the valence band of i-$Al_{65}Cu_{20}Ru_{15}$ (Fig. 2) consists of two overlapping peaks and a broad spectral weight around $E_B = -5$ eV. The two peaks must be predominantly due to the Ru 4d and the Cu 3d states because the Al sp spectral contribution is expected to be much smaller due to the small photoionization cross section for Al sp orbitals for the photon energies used here (Fig. 3).[85] In order to identify unambiguously the origin of these two features, photoemission spectra were measured at different photon energies.

1. *Resonant photoemission data*

To establish the main features in a valence band due to the Ru 4d states, a resonant photoemission effect can be employed.[86] In this effect the ionization cross section of an outershell electron is enhanced as the excitation energy exceeds the threshold of an inner excitation. For TM elements the resonance occurs at excitation energies near the np and nf threshold, which for the Ru $4p \rightarrow 4d$ transition in a Ru metal is expected to occur at about 43.2 eV ($4p_{3/2} \rightarrow 4d$) and 46.5 eV ($4p_{1/2} \rightarrow 4d$). Resonance photoemission for Ru-containing alloys involves two processes. The first process is the direct excitation,

$$4p^6 4d^7 + h\nu \rightarrow 4p^6 4d^6 \varepsilon_f \ . \quad (1)$$

The other involves a 4p core excitation followed by a super-Coster-Kronig decay,

$$4p^6 4d^7 + h\nu \rightarrow 4p^5 4d^8 \rightarrow 4p^6 4d^6 \varepsilon_f \ . \quad (2)$$

The final states obtained via these two processes are indistinguishable, so that there is a quantum interference between the two processes. As a result, the Ru 4d-derived features are enhanced or suppressed as the photon energy is swept through the 4p-4d threshold. It can be seen in Fig. 4 that, as the photon energy increases, the intensity of the $E_B = -1.3$ eV feature decreases first and reaches its first minimum at $h\nu = 43$ eV. Then it increases slightly between $h\nu = 44$ and 46 eV. It decreases slightly again at $h\nu = 47$ eV and starts to increase for higher photon energies. This indicates that this feature is predominantly due to the Ru 4d-derived states.

Another way of performing a resonance photoemission experiment, which shows more clearly the photoemission intensity variations due to resonance, is to measure, or calculate from the PES spectra obtained for different photon energies, the so-called constant-initial-state (CIS) spectra.[86,87] These spectra represent the dependence of the photoemission intensity on the photon energies for selected valence-band positions identified by their initial energy E_i. Such CIS spectra for the E_i values corresponding to the positions denoted by A, B, C, and D in Fig. 4 are shown in Fig. 5. One can see a minimum for photon energies around 43 eV, and another weak and not resolved minimum for photon energies around 47 eV.

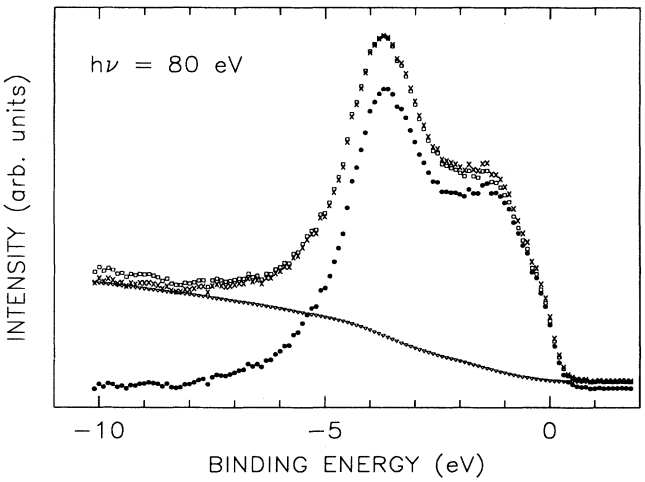

FIG. 2. Effect of the secondary-electron contribution on the valence-band spectrum of i-$Al_{65}Cu_{20}Ru_{15}$ measured at a photon energy $h\nu = 80$ eV. (□)—the as-measured spectrum, (×)—the analyzer and flux-corrected as-measured spectrum scaled to the most intense peak of the as-measured spectrum, (▽)—secondary-electron contribution to the analyzer- and flux-corrected as-measured spectrum, (●)—resultant spectrum after subtraction of the secondary-electron contribution.

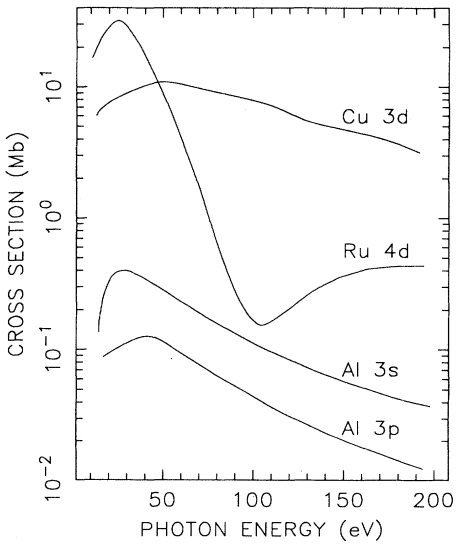

FIG. 3. Atomic subshell photoionization cross sections as a function of photon energy for Cu 3d, Ru 4d, Al 3s, and Al 3p orbitals. Data are taken from Ref. 85. Note the logarithmic scale on the ordinate axis.

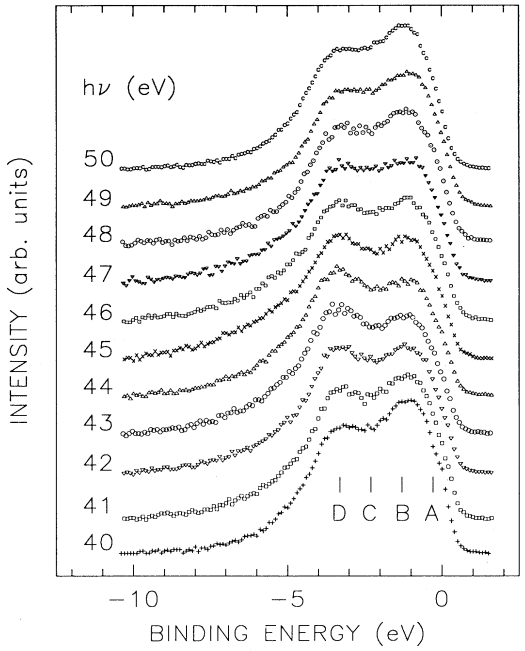

FIG. 4. Valence-band spectra of i-$Al_{65}Cu_{20}Ru_{15}$ for different photon energies around the Ru $4p \rightarrow 4d$ transition. *A*, *B*, *C*, and *D* identify binding energies for which CIS spectra were measured (Fig. 5).

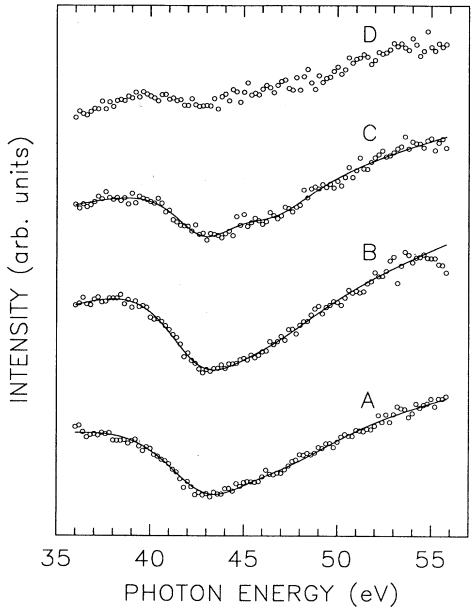

FIG. 5. Constant-initial-state (CIS) spectra measured for the valence-band positions *A*, *B*, *C*, and *D* in Fig. 4, which are identified here by the same letters. The solid line is a fit to two Fano profiles and a linear background, as described in the text and with parameters given in Table II.

The line shape of the resonance resulting from the processes (1) and (2), $I(h\nu)$, can be characterized by the Fano profile,[86,87]

$$I(h\nu)=I_0(h\nu)\frac{(\varepsilon+q)^2}{1+\varepsilon^2}+I_{nr}(h\nu)\ , \tag{3}$$

where $I_0(h\nu)$ is the nonresonant Ru $4d$ emission, $I_{nr}(h\nu)$ is a noninterfering background contribution, q is Fano's asymmetry parameter, and $\varepsilon=2(h\nu-E_R)/\Gamma$ is the reduced energy expressed in terms of the energy, E_R, and width, Γ [full width at half maximum (FWHM)], of the resonance. The experimental CIS spectra (Fig. 5) were fitted to two Fano profiles because of the two Ru $4p \rightarrow 4d$ transitions mentioned above. Due to the strong overlap of the two profiles, these transitions were characterized by the same parameters q and Γ. A linear background $I_{nr}(h\nu)$ was assumed in the fit. The parameters obtained from the fit are given in Table II.

A good fit was obtained (Fig. 5) with the two Fano profiles described above. However, due to the strong overlap of the two broad $4p_{3/2} \rightarrow 4d$ and $4p_{1/2} \rightarrow 4d$ transitions, the fitted parameters are strongly correlated and therefore, caution is required in their physical interpretation. As expected, the nonresonant emission parameters corresponding to the two transitions fulfill the inequality $I_0^{3/2} > I_0^{1/2}$ (Table II). The corresponding resonance energies $E_R^{3/2}$ and $E_R^{1/2}$ (Table II) are close to the core-level values for a Ru metal. The broad character of the resonance is reflected (Table II) in the large values of Γ and the value of q which is close to zero.[86] The strongest resonance occurs for $E_i=-1.3$ eV (Fig. 5 and Table II). There is a very weak resonance for $E_i=-3.3$ eV (Fig. 5, curve *D*), which, however, could not be reliably fitted. The fact that the resonance takes place in a rather broad valence-band region can be interpreted as evidence of hybridization between the Ru $4d$ and the Al sp and/or Cu $3d$ states.

The strong correlation mentioned above between the fitted parameters in Table II makes it difficult to give them a definite physical interpretation. Furthermore, the noninterfering background I_{nr}, which was assumed to be linear, may have a different, and unknown, photon-energy dependence. To avoid these problems, CIS-type spectra can be also generated directly from the valence-band spectra in Fig. 4 by plotting the intensity at a given binding energy versus the photon energy (Fig. 6). The CIS intensity was calculated as an average of five PES intensity values around a given binding energy in order to remove possible height fluctuations due to statistical uncertainties in the measured PES intensity. Although there are much fewer CIS points (limited only by the number of PES spectra measured for different values of $h\nu$) in Fig. 6 as compared to Fig. 5, one can nevertheless observe clearly several effects. First, the two minima at the photon energies 44 ± 1 eV and 47 ± 1 eV corresponding, respectively, to the $4p_{3/2} \rightarrow 4d$ and $4p_{1/2} \rightarrow 4d$ transitions are now separated. This justifies the fit of the CIS

TABLE II. Parameters obtained by fitting two Fano line shapes [Eq. (3)], corresponding to the Ru $4p_{3/2} \rightarrow 4d$ and $4p_{1/2} \rightarrow 4d$ transitions, to the CIS spectra in Fig. 5 for the E_i values corresponding to the positions *A*, *B*, and *C* indicated in Fig. 4. The parameters with the superscripts 3/2 and 1/2 refer, respectively, to the Ru $4p_{3/2} \rightarrow 4d$ and $4p_{1/2} \rightarrow 4d$ transitions.

Spectrum	E_i (eV)	$I_0^{3/2}$	$I_0^{1/2}$	$E_R^{3/2}$ (eV)	$E_R^{1/2}$ (eV)	q	Γ (eV)
A	−0.3	33.3 (1.2)	8.4 (2.0)	42.3 (2)	47.0 (4)	−0.30 (8)	7.1 (4)
B	−1.3	36.5 (1.8)	7.3 (2.8)	42.0 (2)	46.1 (5)	−0.48 (9)	6.6 (5)
C	−2.3	23.7 (9)	11.5 (1.7)	42.4 (2)	46.4(3)	−0.28 (7)	4.9 (4)

spectra in Fig. 5 with two Fano profiles. Second, the strongest resonance enhancement occurs for $E_i = -1.3$ eV, which corresponds to the peak position of one of two features in the PES spectra (Fig. 4). This confirms that the maximum spectral weight due to the Ru 4*d*-derived states is at 1.3 eV below E_F. Third, the amplitude of the resonance decreases as E_i becomes more negative, which means that the spectral weight of the Ru 4*d*-derived states diminishes for lower E_B values. However, a weak resonance is clearly seen for E_B values quite far from E_F (the $E_i = -3.3$ eV curve in Fig. 6). This indicates that the Ru 4*d*-derived states extend far from E_F, probably due to their hybridization with the Al *sp* and/or Cu 3*d* states. We also note that as E_i becomes more negative, the amplitude associated with the $4p_{3/2} \rightarrow 4d$ transition decreases whereas the amplitude corresponding to the $4p_{1/2} \rightarrow 4d$ transition increases; we have at present no explanation of this result. Further experimental evidence in support of the predominantly Ru 4*d* character of the $E_B = -1.3$-eV feature in the valence band of the *i*-$Al_{65}Cu_{20}Ru_{15}$ alloy is given in the next section.

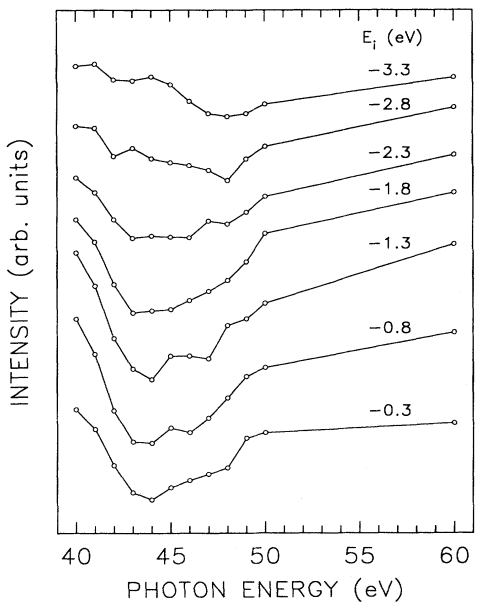

FIG. 6. Constant-initial-state spectra for the indicated values of the initial energy E_i which were generated from the PES spectra of Fig. 4, as described in the text. The straight lines joining the points are guides for the eye.

2. *Photoemission data near the Cooper minimum*

The features in the valence bands originating from the 4*d* and/or 5*d* states in alloys containing the 4*d* and/or 5*d* elements can be identified by making use of the Cooper minimum effect[88] which is the occurrence of a minimum in the photoionization cross section for particular orbitals. This effect results from the presence of a node or nodes in the radial part of the 4*d* and 5*d* (but not 3*d*) atomic wave functions. The Cooper minimum in the Ru 4*d* photoionization cross section is calculated to be at about $h\nu = 105$ eV for a Ru atom[85] (Fig. 3). However, its position and depth are usually changed in alloys due to solid-state effects.[51,88] Since the decrease of the Ru 4*d* photoionization cross section in the 50 to 200-eV photon-energy range is expected to be almost as large as two orders of magnitude (Fig. 3), one can anticipate a strong suppression of the contribution of the Ru 4*d* character to the valence band of *i*-$Al_{65}Cu_{20}Ru_{15}$ for the values of $h\nu$ close to the Cooper minimum.

Figure 7 shows that as $h\nu$ increases from below the Cooper minimum, the relative contribution of the $E_B = -1.3$-eV feature with respect to the other feature originating from the Cu 3*p*-derived states first decreases, reaches its minimum at $h\nu = 130$ eV, and then starts to increase for higher photon energies. Note that the Cooper minimum effect is much more dramatic (Fig. 7) than the Ru $4p \rightarrow 4d$ photoemission resonance effect (Fig. 4). To present the Cooper minimum effect in a more quantitative way, a plot of the photoemission intensity at $E_B = -1.3$ eV as a function of $h\nu$ is presented in Fig. 8. This intensity was calculated as an average of 11 intensity values around $E_B = -1.3$ eV. One can see clearly a strong decrease of the photoemission intensity with increasing photon energy. However, the minimum is not at 105 eV (Fig. 3) but is shifted to 130 eV. As mentioned above, this shift is caused by the solid-state effects.[51,88]

The contribution due to the Cu 3*d*-derived states is well separated for $h\nu = 130$ eV from the contribution originating from the Ru 4*d*-derived states (Fig. 7), and has its peak at $E_B = -3.8$ eV. The weak and broad spec-

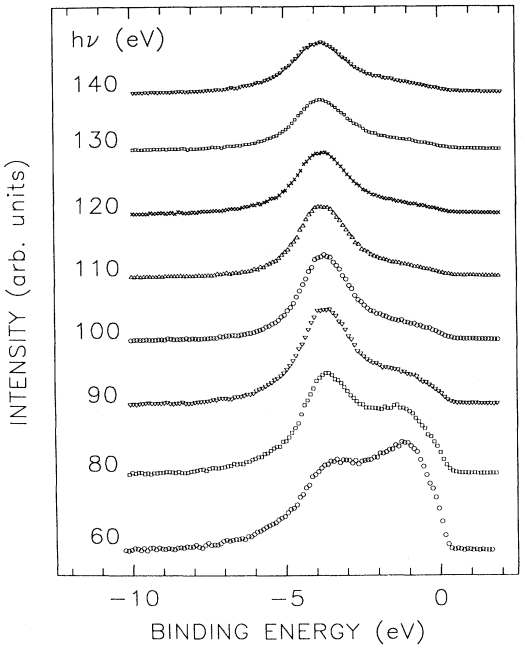

FIG. 7. Valence-band spectra of i-$Al_{65}Cu_{20}Ru_{15}$ for different photon energies around the Ru 4d Cooper minimum.

tral weight around $E_B = -5$ eV can be ascribed to the Al sp-derived states, based on the results of the SXE studies of i-Al-based alloys.[45]

It is now widely accepted that PES valence bands measured typically for $h\nu \geq 40$ eV (XPS regime) represent the initial DOS weighted by frequency-dependent dipole matrix elements and by the photon energy-dependent photoionization cross sections, σ, for various s, p, d, and f states.[89] To a good approximation, it can be assumed that the matrix elements change little over the width of the valence band. Thus the measured PES valence bands, when properly corrected for the experimental factors and the inelastically scattered electrons, are generally proportional to the DOS modulated by the photoionization cross sections. In the particular case of the studied i-$Al_{65}Cu_{20}Ru_{15}$, the valence bands measured for $h\nu$ values outside the Ru $4p \rightarrow 4d$ resonance and the Ru Cooper minimum, and for which the Cu 3d and Ru 4d photoionization cross sections are about the same, are expected to represent well the total DOS of d character. Since $\sigma_{Ru} \approx \sigma_{Cu}$ at $h\nu = 80$ eV (note that Fig. 8 indicates that the theoretical Ru 4d curve in Fig. 2 is shifted in the studied compound by about 25 eV to the higher $h\nu$ values), the valence band measured at that photon energy (Fig. 7) should represent well the total d-derived DOS in the studied alloy. Additional arguments supporting this conclusion will be given below.

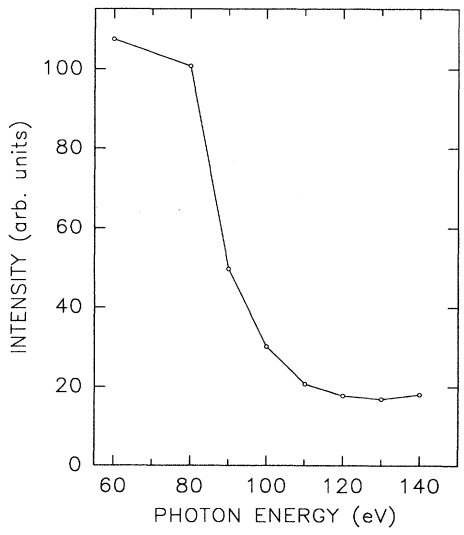

FIG. 8. Photoemission intensity at the binding energy of −1.3 eV as a function of photon energy obtained from the spectra in Fig. 7, as described in the text. The solid line is a guide for the eye.

Note that for the photon-energy range used in this study, $\sigma_{Cu}(h\nu)$ varies slowly with $h\nu$ (Fig. 3), whereas the changes of $\sigma_{Ru}(h\nu)$ with $h\nu$ are much more dramatic (Figs. 3 and 8). This is nicely reflected in the measured valence bands. For $h\nu$ range between 50 and 60 eV and outside the $4p \rightarrow 4d$ resonance, where $\sigma_{Cu}(h\nu) < \sigma_{Ru}(h\nu)$ (as noted before, the theoretical Ru 4d curve in Fig. 3 should be shifted by 25 eV to higher $h\nu$ values), the intensity of the features due to the states of the Cu 3d character is smaller than the intensity of the feature due to the states of the Ru 4d character (Figs. 4 and 7). For $h\nu$ values larger than 60 eV, where $\sigma_{Cu}(h\nu) > \sigma_{Ru}(h\nu)$ (Fig. 3), this intensity ratio is reversed (Fig. 7).

D. Partial DOS due to Ru 4d- and Cu 3d-derived states

The analysis presented above allowed us to unambiguously ascribe the two main features in the valence band of i-$Al_{65}Cu_{20}Ru_{15}$ to the Ru 4d- and Cu 3d-derived states. To determine the experimental electronic structure associated with the occupied energy levels of an alloy, it is also necessary to establish partial spectral weights associated with s, p, d, and f states of a given element in the alloy. These partial weights are generally proportional to the partial DOS associated with a given state of that element, as was explained above. Before the advent of synchrotron radiation as a tunable excitation source, such partial DOS was determined almost exclusively using the SXE technique. The use of synchrotron-radiation-based PES technique allows one also to determine such partial DOS, as is demonstrated below.

PES valence bands represent mainly the DOS of the d and/or f character because the σ values corresponding to the d and f orbitals are significantly larger than the corresponding values associated with the s and p orbitals (Ref. 85 and Fig. 3). Thus the contribution to the valence band of i-$Al_{65}Cu_{20}Ru_{15}$ due to sp states can be neglected. The intensity $I(h\nu, E_B)$ of the valence-band PES spectrum of i-$Al_{65}Cu_{20}Ru_{15}$ at binding energy E_B and incident photon energy $h\nu$ can be represented[90] by

$$I(h\nu,E_B)=C(h\nu)[\sigma_{Cu}(h\nu)D_{Cu}(E_B)/Z_{Cu} + \sigma_{Ru}(h\nu)D_{Ru}(E_B)/Z_{Ru}] , \quad (4)$$

where D_i is the partial DOS of the ith element (i=Cu, Ru). The partial DOS is assumed to fulfill the normalization condition,

$$\sum D_i(E_B)\Delta E_B = N_i Z_i , \quad (5)$$

where N_i and Z_i are, respectively, the concentration and the number of d electrons of the ith element. We have $N_{Cu}=0.20$, $N_{Ru}=0.15$, and assume that $Z_{Cu}=10$ and $Z_{Ru}=7$. The instrumental factor is represented by $C(h\nu)$. In principle, this factor should be independent of $h\nu$ if the corrections of the *as*-measured valence bands, which are described in Sec. III B, could be done ideally and if one could know precisely the values of $\sigma_{Cu}(h\nu)$ and $\sigma_{Ru}(h\nu)$ in the studied alloy. Since, in practice, this cannot be achieved, the factor $C(h\nu)$ has a weak dependence on $h\nu$.

For compounds containing a d- or f-electron element for which a Cooper minimum or resonance photoemission effects can be observed, it has been standard practice to use a difference between the valence bands, respectively, away and at the Cooper minimum,[88,91] or on- and off-resonance,[91,92] to determine the partial DOS of that element. Such a difference spectrum enhances the d or f contribution of that element to the valence band because of the strong variation of the d- and f-like spectral weight for $h\nu$ values close to the values at which Cooper minimum or resonance photoemission occur, and because the changes of the σ values with $h\nu$ of the orbitals of other elements of an alloy are usually negligibly small, and thus cancel out.

In order to assess the reliability and the reproducibility of the Ru 4d partial DOS in i-$Al_{65}Cu_{20}Ru_{15}$ represented by the difference spectrum, the latter was evaluated in several ways. We used first the valence-band spectra for the $h\nu$ values around the Copper minimum (Fig. 7). A difference spectrum obtained by direct subtraction of the $h\nu$=130-eV spectrum from the $h\nu$=60 eV, which is equivalent to the assumption that $C(h\nu)$ and $\sigma_{Cu}(h\nu)$ in Eq. (4) are independent of $h\nu$, is shown by filled circles in Fig. 9. Next the difference between the same valence-band spectra was calculated by scaling the $h\nu$=60-eV spectrum to match the height of its Cu 3d feature to that of the $h\nu$=130-eV spectrum (curve marked with the × symbols in Fig. 9); this is a graphical attempt to account for the differences between the $\sigma_{Cu}(h\nu)$ values at $h\nu$=60 and 130 eV. One can see (Fig. 9) that this height scaling produces an unphysical negative peak around $E_B=-4$ eV, and, therefore, this scaling procedure was rejected in further analysis. It can be noted that this unphysical negative peak results from the overestimation of the height of the Cu 3d feature in the $h\nu$=60 eV caused by the overlap with the neighboring Ru 4d feature. The third way of calculating the difference spectrum was based on scaling the $h\nu$=60-eV spectrum according to the theoretical [(Ref. 85) and Fig. 3] photoionization cross-section ratio and subtracting from it the $h\nu$=130-eV spectrum (curve marked with ∇ symbols in Fig. 9). One can notice again

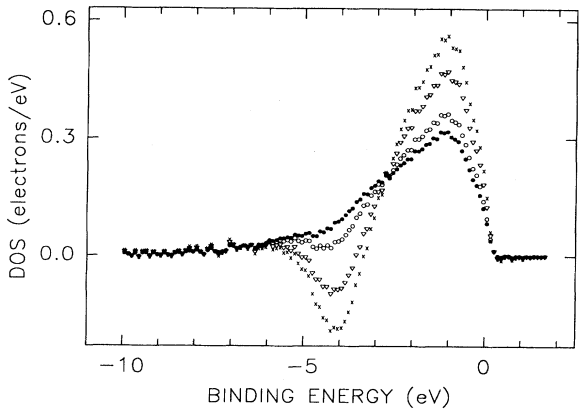

FIG. 9. Difference between the $h\nu$=60-eV and $h\nu$=130-eV spectra from Fig. 7 obtained by a direct subtraction (●), by a subtraction following the scaling to the Cu 3d peak of the two spectra (×), by a subtraction following the scaling according to $\sigma_{Cu}(h\nu)$ values from Ref. 85 (∇), and by subtraction following the scaling to the modified $\sigma^a_{Cu}(h\nu)$ values (○), as described in the text.

an unphysical negative peak around $E_B=-4$ eV (Fig. 9), which indicates that $\sigma_{Cu}(h\nu)$ in the studied alloy decreases more slowly with $h\nu$ than predicted by theory.[85] The weaker dependence of $\sigma_{Cu}(h\nu)$ on $h\nu$ is also expected from the lack of a negative peak in the difference spectrum obtained with the direct subtraction method. One can eliminate this negative peak by assuming that the Cu 3d photoionization cross section, $\sigma^a_{Cu}(h\nu)$, in the studied alloy changes with $h\nu$ according to the relation $\sigma^a_{Cu}(h\nu)=\sigma_{Cu}(h\nu)+0.03(h\nu-50)$, where $\sigma_{Cu}(h\nu)$ is the theoretical value calculated by Yeh.[85] The difference spectrum obtained with the corrected $\sigma^a_{Cu}(h\nu)$ values (open circles in Fig. 9) does not have a negative peak and is quite similar to the spectrum calculated by the direct subtraction method. It can be concluded that all four methods of calculating the difference spectrum give essentially the same position 1.2(1) eV for the maximum of the Ru 4d partial DOS (Fig. 9). The direct subtraction method and the method based on scaling according to the corrected $\sigma^a_{Cu}(h\nu)$ values lead to essentially the same Ru 4d partial DOS. The other two methods produce unphysical negative peaks and are, therefore, not reliable.

The Ru 4d partial DOS determined by the subtraction method should not depend on the choice of the two valence-band spectra used in this method. As an example, Fig. 10(a) presents the difference spectra obtained with the direct subtraction method and with the method based on scaling according to the corrected $\sigma^a_{Cu}(h\nu)$ values calculated in the same way as described above, but for the two spectra from Fig. 7 measured at $h\nu$=80 and 90 eV. A comparison of these difference spectra with the corresponding spectra obtained from the $h\nu$=60 and 130 eV valence bands, which for convenience of comparison are replotted in Fig. 10(b), shows that their shapes, widths, and the locations of the peak maximum, apart from the expected minor differences, are very similar. And finally, the above two subtraction methods, when applied to the valence bands (Fig. 4) measured on-

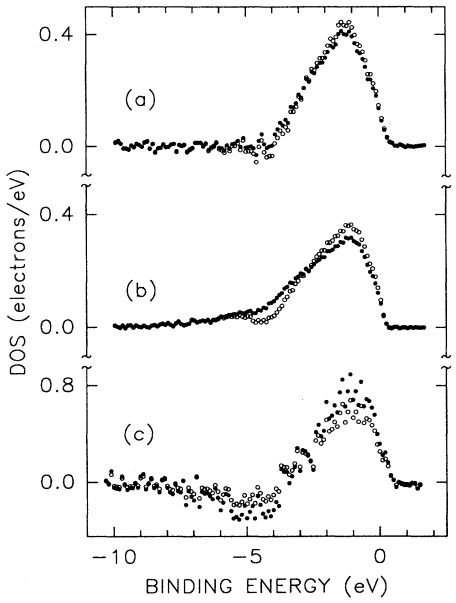

FIG. 10. Difference spectra obtained from the valence bands in Figs. 4 and 7 by the direct subtraction method (●) and by the subtraction method based on scaling according to the modified $\sigma^a_{Cu}(h\nu)$ values (○), as described in the text. The difference spectra are calculated for valence bands measured at (a) $h\nu=80$ and 90 eV, (b) $h\nu=60$ and 130 eV, and (c) $h\nu=41$ and 44 eV.

resonance ($h\nu=41$ eV) and off-resonance ($h\nu=44$ eV) highlight the Ru 4*d* partial DOS [Fig. 10(c)]. Apart from being more scattered due to the smaller intensity changes in the resonant PES valence bands as compared to the corresponding changes close to the Cooper minimum, this Ru 4*d* partial DOS [Fig. 10(c)] is very similar to the ones in Figs. 10(a) and 10(b). We can thus conclude that the Ru 4*d* partial DOS extends from E_F to 4.5(2) eV below E_F, has its maximum intensity at the $E_B=1.3(1)$ eV, and the FWHM of 2.8(3) eV.

The subtraction methods described above are based on the assumption of the independence of the $C(h\nu)$ factor in Eq. (4) of $h\nu$ and were used to determine the partial DOS of Ru 4*d* character. We concentrated on the Ru 4*d* partial DOS as its contribution to the DOS(E_F), as is shown below, is more significant than that associated with the Cu 3*d* states. In order to determine both the partial DOS of the Ru 4*d*-derived states and of the Cu 3*d*-derived states, Eq. (4) is used for two different $h\nu$ values, and the factors $C(h\nu)$ corresponding to these values are then determined from the total integrated intensity of the experimental valence bands, the normalization condition of Eq. (5), and the values of $\sigma_{Cu}(h\nu)$ and $\sigma_{Ru}(h\nu)$. The Cu 3*d* and Ru 4*d* partial DOS obtained in this way by using the $h\nu=60$ and 130 eV valence bands from Fig. 7, as well as their sum, are shown in Fig. 11. The Ru 4*d* partial DOS (Fig. 11) agrees well with that determined with the subtraction methods (Fig. 10).

Using Eq. (4), one should be able to reproduce the experimental valence bands measured for all $h\nu$ values provided that the Cu 3*d* and Ru 4*d* partial DOS in Fig. 11 are a good measure of the true Cu 3*d* and Ru 4*d* DOS in *i*-$Al_{65}Cu_{20}Ru_{15}$ and provided that the $\sigma_{Cu}(h\nu)$ and $\sigma_{Ru}(h\nu)$ values are accurate enough. The reproduced valence bands calculated for all $h\nu$ values are compared with the corresponding experimental valence bands in Fig. 12. Obviously, there is a perfect agreement (Fig. 12) between the experimental valence bands measured at $h\nu=60$ and 130 eV and the corresponding generated bands since these two experimental valence bands were used to determine the Cu 3*d* and Ru 4*d* partial DOS of Fig. 11. Keeping in mind the simplicity of the model expressed by Eq. (4), there is a reasonably good agreement between the predictions of the model and the experimental data (Fig. 12).

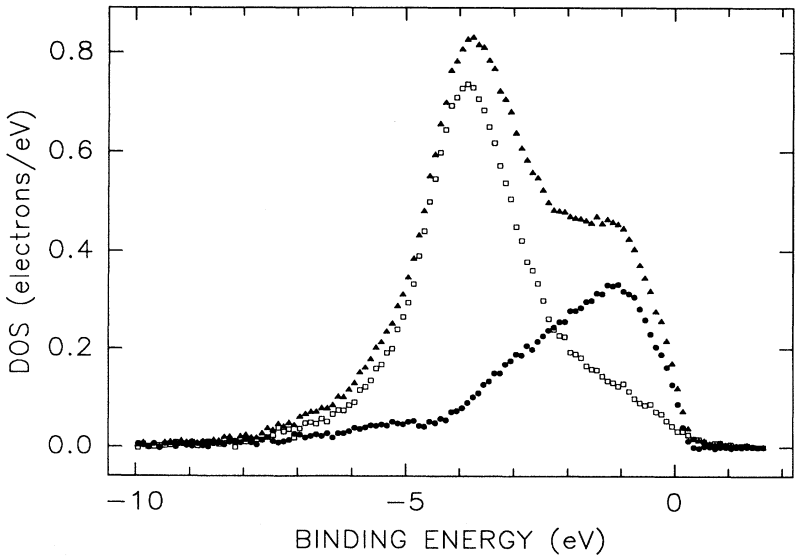

FIG. 11. Partial DOS of the Cu 3*d*-derived state (□) and the Ru 4*d*-derived states (●) obtained from the $h\nu=60$ and 130-eV valence bands in Fig. 7 and by using Eq. (4), as described in the text. Their sum (▲) represents the total DOS of *d* character in *i*-$Al_{65}Cu_{20}Ru_{15}$.

E. Minimum of DOS (E_F) and DOS spikiness in quasicrystals: Theory and experimental evidence

It would be useful to compare the valence band of *i*-$Al_{65}Cu_{20}Ru_{15}$ with that of a corresponding crystalline alloy. No ternary alloys in the Al-Cu-Ru system were known until recently when Shield *et al.*[60] discovered two approximant phases in this system. Also no theoretical calculations of the DOS in an approximant of the *i*-$Al_{65}Cu_{20}Ru_{15}$ alloy have been performed yet, so we cannot compare our empirically determined DOS and the Cu 3*d* and Ru 4*d* partial DOS (Fig. 11) with theory. We, therefore, compare the valence band of *i*-$Al_{65}Cu_{20}Ru_{15}$ with the valence bands of constituent elements (Fig. 13). One can notice (Figs. 11 and 13) a clear shift of the Cu 3*d* spectral weight in the studied alloy away from E_F as compared with the corresponding spectra weight in pure Cu. Such a shift is expected to result in a decrease of the Cu 3*d* contribution to the DOS (E_F). A similar shift is not observed for the Ru 4*d* spectral weight (Figs. 11 and 13) and, consequently, one can anticipate a Ru 4*d* contribution to the DOS (E_F) which is not negligible. The Al *sp* states are expected to spread throughout the valence band (Fig. 13), but cannot be detected in the measured spectra due to the small σ values associated with the Al *s* and *p* orbitals (Ref. 85 and Fig. 3). As mentioned before, the Al *sp*-derived states are manifested as a broad spectral weight around $E_B = -5$ eV, where the contributions from the Cu 3*d*- and Ru 4*d*-derived states are relatively small.

When the valence band of *i*-$Al_{65}Cu_{20}Ru_{15}$ is compared with the valence bands of two other thermodynamically stable *i* alloys, $Al_{65}Cu_{20}Fe_{15}$ and $Al_{70}Pd_{20}Mn_{10}$ (Fig. 14), two common characteristics stand out. First, the Cu 3*d*- and Pd 4*d*-derived features are pushed away from E_F in comparison to their locations in pure Cu and Pd metals, whereas the features associated with the Ru 4*d*-, Fe 3*d*-, and Mn 3*d*-derived states remain close to E_F. Thus one would expect a relatively small contribution to the DOS (E_F) from the Cu 3*d*- and Pd 4*d*-like states and a nonnegligible contribution due to the Ru 4*d*-, Fe 3*d*-, and Mn 3*d*-like states (Fig. 11). Second, there is a strong depression of the PES intensity as the energy approaches E_F.

The depression of intensity as the energy approaches E_F observed in the PES (Refs. 39, 41, and 48) and SXE

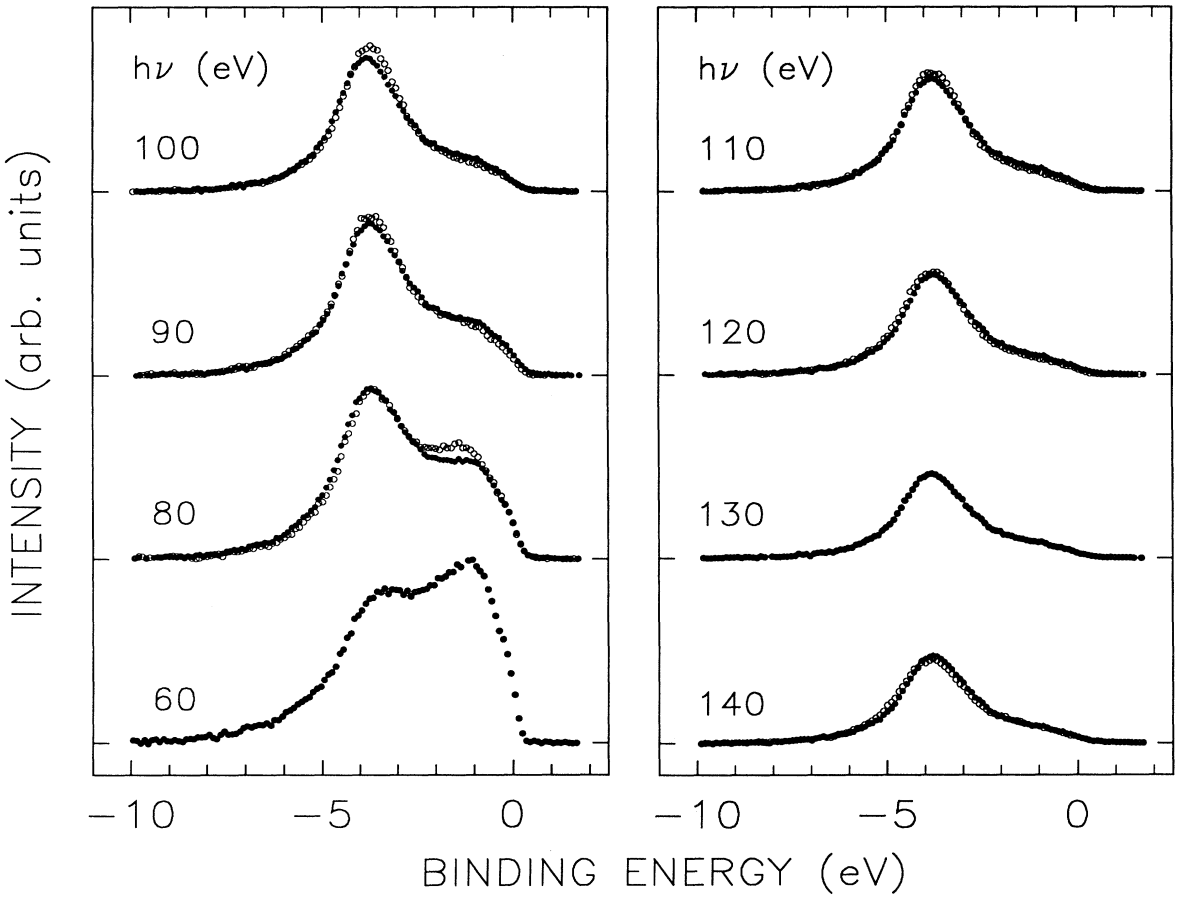

FIG. 12. Comparison of the valence bands generated from Eq. (4) using the empirical partial Cu 3*d* and Ru 4*d* DOS of Fig. 11 (●) with the experimental valence bands from Fig. 7 (○).

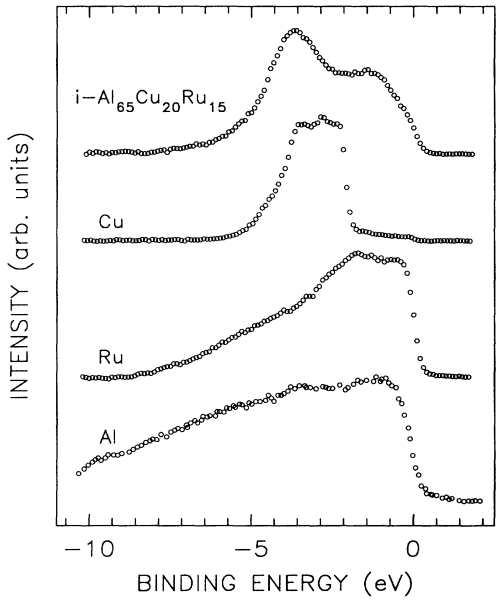

FIG. 13. Comparison of the PES valence band of i-$Al_{65}Cu_{20}Ru_{15}$ with that of Cu metal (the raw PES spectrum of Cu was kindly provided by T.-U. Nahm and S.-J. Oh; the secondary-electron contribution was subtracted from the original spectrum), Ru metal, and with the XPS valence band of Al obtained from Fig. 2 of Ref. 93. The first three valence bands were measured at $h\nu=80$ eV. The spectra were normalized to give a constant height between the maximum and minimum recorded count.

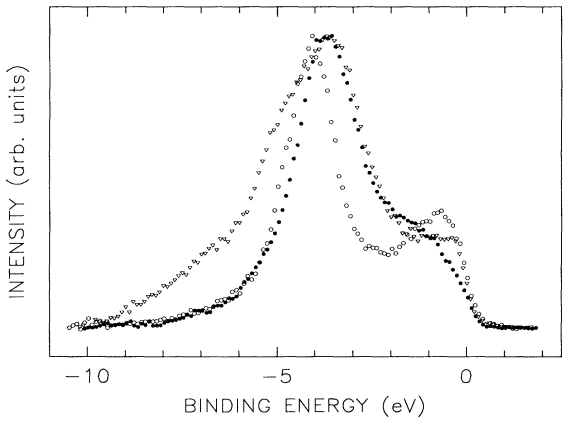

FIG. 14. Valence bands of i-$Al_{65}Cu_{20}Ru_{15}$ (●), i-$Al_{65}Cu_{20}Fe_{15}$ (○), and i-$Al_{70}Pd_{20}Mn_{10}$ (▽) measured, respectively, at $h\nu=90$, 100, and 100 eV. The raw spectrum of i-$Al_{65}Cu_{20}Fe_{15}$ from Ref. 48 has been corrected for the energy dependence of the electron transmission of the electron-energy analyzer, normalized for the photon flux, and corrected for the secondary-electron background. The spectrum of i-$Al_{70}Pd_{20}Mn_{10}$ is from Ref. 51. The spectra were normalized to give a constant height between the maximum and minimum recorded count.

(Refs. 42–47, and 49) spectra of the QC's containing TM elements, and also observed here (Figs. 4, 7, 9–11, 14), has been interpreted as evidence for the opening of a theoretically predicted[21–25] pseudogap at E_F. Such an interpretation, however, is open to criticism because there are two effects which lead to the intensity decrease as the energy approaches E_F. The first one is a simple Fermi cutoff,[40,51] which would be especially important for the QC's with TM elements whose d states, as was demonstrated in this work, significantly contribute to the measured intensity around E_F. In the case of the studied i-$Al_{65}Cu_{20}Ru_{15}$, the Ru $4d$-derived states do contribute to the measured intensity at E_F (Figs. 9–11). The second effect leading to the decrease of intensity as the energy approaches E_F could be associated with the opening of a pseudogap in the vicinity E_F. We are only able to conclude that our PES results are indicative of a possible opening of a pseudogap at E_F in i-$Al_{65}Cu_{20}Ru_{15}$, but they do not prove its existence. As we shall argue below, high-energy resolution PES and/or SXE experiments are essential for obtaining definite experimental evidence for the possible existence of such a pseudogap.

The separation of the above two effects, and thus an unambiguous experimental verification of the existence of the theoretically predicted pseudogap, is possible only when high-resolution PES and/or SXE experiments, preferably combined with the corresponding IPES and/or SXA measurements, are conducted. performed so far had an energy resolution, which is dependent on the photon energy used, between 0.3 and 0.7 eV,[39,41,43,48,51] with the exception of one PES study conducted with the energy resolution of 0.14 eV.[39] The only IPES study reported so far had an energy resolution of 0.7 eV.[43] The SXE and SXA studies previously reported had an energy resolution, which is dependent on the element considered, in the range 0.2–0.7 eV,[38,42,43,46,47] and a relatively high uncertainty (0.1–0.3 eV) associated with the determination of the position of E_F. We believe that these energy resolutions are not high enough, and for the SXE/SXA studies the uncertainty in determining the location of E_F is too big to warrant the claims of the definite spectroscopic verification of the existence of a pseudogap at E_F. The arguments given below support this statement.

In a recent study, the electronic structure[94] of the hypothetical 1/1 cubic approximant[95] to the icosahedral Al-Cu-Fe phase has been calculated. The model approximant of composition $Al_{80}Cu_{32}Fe_{16}$ consisted of 128 atoms in a simple cubic cell with a lattice constant of 12.30 Å.[94] Its total DOS, which was kindly provided to us by Fujiwara,[94] is presented in Fig. 15. It should be noticed first that there are three features in the theoretical DOS located at about 1.0, 1.9, and 3.9 eV below E_F which correspond, respectively, to the Fe $3d$-, Al $3p$-, and Cu $3d$-derived states.[94] The Fe $3d$ and Cu $3d$ features are clearly seen in the experimental valence band of i-$Al_{65}Cu_{20}Fe_{15}$ (Fig. 14), whereas the Al $3p$ feature is suppressed because of the small σ value of the Al $3p$ orbitals (Fig. 3). Of more importance for the present discussion, however, is the presence of a pseudogap of the width of about 0.5 eV whose center is located at about 0.3

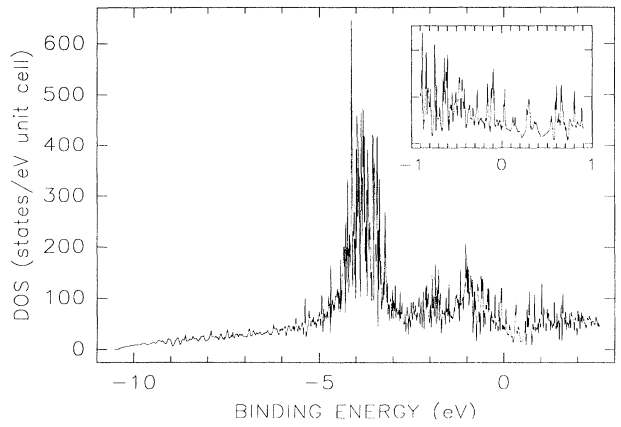

FIG. 15. Total electronic density of states for the 1/1 icosahedral approximant $Al_{80}Cu_{32}Fe_{16}$ from Ref. 94. The inset shows a part of the DOS around E_F. The energy mesh of 0.001 Ry was used to calculate the DOS shown in the figure, and of 0.0001 Ry—for the DOS shown in the inset (Ref. 94). The three ticks on the ordinate axis of the inset correspond, respectively, to 0, 100, and 200 states/eV unit cell.

eV above E_F (inset in Fig. 15). Obviously, such a pseudogap cannot be detected using the PES and/or SXE techniques with the energy resolutions mentioned above.

In order to make a comparison between a theoretical DOS and the experimental valence band more meaningful, the former has to be appropriately broadened to account for all its known distortions introduced by the measurement. Among them, the two most important broadening effects are the lifetime broadening described by a Lorentzian with HWHM in the form $\Gamma_L^0(|E_B|-E_F)^2$, where Γ_L^0 is a parameter which fixes the scale of the broadening, and the instrumental broadening which is usually represented by a Gaussian with FWHM, Γ_G, equal to the energy resolution of the experiment.[96] The left panel of Fig. 16 shows the influence on the theoretical DOS from Fig. 15 of only the instrumental broadening (the influence of the Fermi-Dirac distribution function at room temperature, which was taken into account, is negligibly small) for the Γ_G values ranging from 0.4 eV, which corresponds to a typical energy resolution of a PES experiment, down to the value of 0.025 eV, which is close to the best PES energy resolution that can

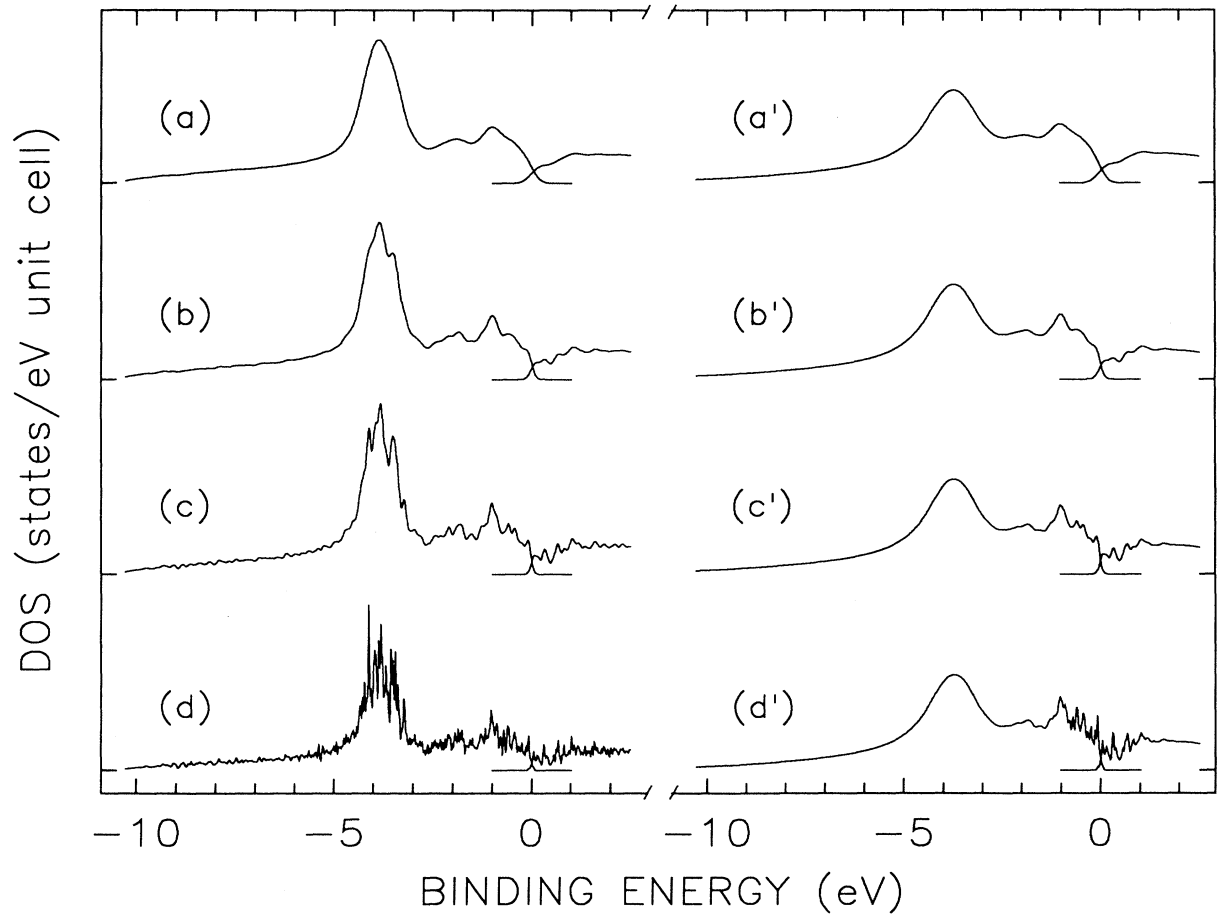

FIG. 16. Left panel: DOS from Fig. 15 convoluted with a Gaussian of the FWHM equal to (a) 0.4 eV, (b) 0.2 eV, (c) 0.1 eV, and (d) 0.025 eV. Right panel: DOS from Fig. 15 convoluted with a Lorentzian of the HWHM equal to $\Gamma_L^0(|E_B|-E_F)^2$, where $\Gamma_L^0=0.025$ eV^{-1}, and with a Gaussian of the FWHM equal to (*a'*) 0.4 eV, (*b'*) 0.2 eV, (*c'*) 0.1 eV, and (*d'*) 0.025 eV. The separation between the two neighboring ticks on the ordinate scale corresponds to 380 states/eV unit cell, and the DOS values in plot (d) were divided by the factor 1.47.

be currently achieved.[97] The DOS below and above E_F were broadened separately. It can be seen from Fig. 16 that because the pseudogap is located above E_F, it induces a very narrow drop of the spectral weight just before E_F which can be detected only by using a PES measurement of the highest-energy resolution. In view of this, the claim of detecting a "diplike anomaly"[39] at E_F in i-$Al_{65}Cu_{21}Fe_{14}$ seems to be unwarranted. Since the energy resolution of the SXE experiments is significantly lower than that of the PES experiments, it is impossible to make any definite conclusion about the existence of such a pseudogap from the SXE studies alone.

The right panel of Fig. 16 shows the DOS from Fig. 15 multiplied by the Fermi-Dirac distribution function at room temperature and convoluted first with a Lorentzian and then with a Gaussian for the same Γ_G values as those used in the left panel. The Γ_L^0 parameter was fixed to 0.025 eV^{-1} since for this value one obtains good agreement between the widths of the Cu 3d feature of the experimental spectrum of i-$Al_{65}Cu_{20}Fe_{15}$ (Fig. 14) and of the corresponding feature in Fig. 16(a'). The inclusion of the lifetime broadening does not significantly change the DOS in the vicinity of E_F, but has a profound effect on the sharp features located farther away from E_F. One can thus conclude that the high-energy resolution of the PES and SXE experiments is essential if we are to verify unambiguously the possible existence of a pseudogap around E_F in QC's. It can be added here that high-energy-resolution PES was instrumental in the *direct* observation of the superconducting gap in high-T_c superconductors,[98] the pseudogap in the charge-density-wave systems,[99] the structure-induced pseudogap in liquid and amorphous alloys,[52] or the pseudogap in some fullerens.[100] Naturally, the most credible evidence for the possible existence of a pseudogap at E_F in QC's can be obtained by combining the high-energy-resolution PES and IPES, or SXE and SXA experiments.

As mentioned in the Introduction, the predicted pseudogap at E_F in QC's is a generic, but not a specific property distinguishing QC's from the periodic or aperiodic materials. A property which seems to be specific only to QC's is the spikiness of their DOS (Refs. 22–24, and 94) (Fig. 15). This spikiness is associated with a large number of nondegenerated flat bands in QC's and the presence of TM elements in QC's results in its amplification.[94] The width of a spiky peak is of the order of 0.01–0.02 eV (Refs. 22 and 94) (Fig. 15). The valence bands of i-$Al_{65}Cu_{20}Ru_{15}$ presented here show no evidence for the presence of such spikes. These spikes have also not been detected in the PES, IPES, SXE, and SXA experiments performed so far.[4,5,37–51] There are at least two possible explanations of the failure to detect those spikes in experiment. As Fig. 16 clearly indicates, the spikiness is smeared out completely for typical PES and SXE energy resolutions. It is expected to be preserved, and only in the vicinity of E_F, for the energy resolutions better than about 0.1 eV (Fig. 16). The second explanation invokes the possibility of the presence of the chemical and topological disorder in the QC's of high structural quality, which was mentioned in the Introduction. Such a disorder can wash out the spikiness of DOS induced by quasiperiodicity. This section can be concluded with the statement that high-energy-resolution (<0.1 eV) spectroscopic experiments are indispensable for the detection of the predicted pseudogap around E_F and the spikiness of DOS in QC's.

F. Al 2p chemical shift

The Al 2p core-level lines in Al metal and in i-$Al_{65}Cu_{20}Ru_{15}$ are compared in Fig. 17. It can be noticed that the Al $2p_{1/2}$ and $2p_{3/2}$ are separated in the Al metal (inset in Fig. 17), but they overlap in the i-$Al_{65}Cu_{20}Ru_{15}$ alloy. The separation of the Al $2p_{1/2}$ and $2p_{3/2}$ components in the Al metal found from the fit with the two Doniach-Šunjić[101] profiles convoluted with a Gaussian (inset in Fig. 17) is 0.41(1) eV, which is in a good agreement with the value of 0.42 eV reported in the literature.[102] The Gaussian FWHM obtained from the fit was 0.417(7) eV. This, together with the observation of the Al $2p_{1/2}$ and $2p_{3/2}$ components in the Al metal, confirms that the overall energy resolution of the measured PES spectra is about 0.4 eV. The main result obtained from Fig. 17 is the observation of the E_B shift in i-$Al_{65}Cu_{20}Ru_{15}$ by 0.31(2) eV towards lower absolute E_B values with respect to Al metal.

There are only a few reports of shifts of the core-level lines in QC's with respect to pure elements and/or to other crystalline alloys. Ederer *et al.*[5] reported the chemical shifts of 0.2 eV between the Al-Mn alloys of different crystal structure and pure Al, and of less than 0.1 eV between the Al-Mn alloys of crystalline and icosahedral structure. Matsubara *et al.*[40] found a 0.4-eV shift of the Al 2p and Li 1s lines towards higher absolute E_B values in i-$Al_{55}Li_{35.8}Cu_{9.2}$ with respect to the Frank-Kasper crystalline alloy $Al_{54}Li_{36.8}Cu_{9.2}$. The absolute E_B shift of the Al 2p line in i-$Al_{70}Pd_{20}Mn_{10}$ with respect to a pure Al metal reported by Zhang *et al.*[51] was 0.27(10) eV. The

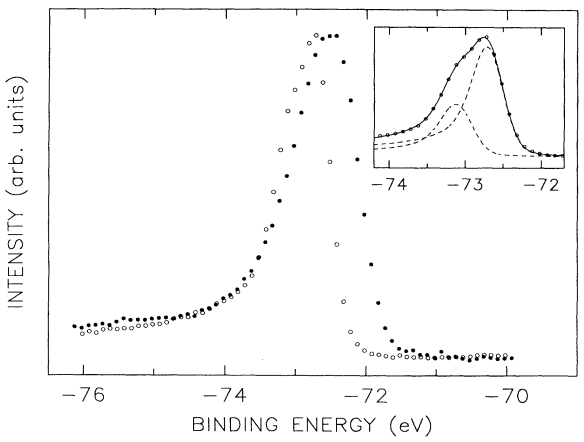

FIG. 17. Al 2p photoemission spectra of the Al metal (○) and i-$Al_{65}Cu_{20}Ru_{15}$ alloy (●) measured at $h\nu=100$ eV. The spectra were normalized to give a constant height between the maximum and minimum recorded count. The inset shows the fit of the Al 2p spectrum of the Al metal with two component Doniach-Šunjić profiles convoluted with a Gaussian, which are also shown, corresponding to Al $2p_{1/2}$ and $2p_{3/2}$ core levels.

values of the observed shifts are small and are comparable to those observed in crystalline alloys.[103] The interpretation of the E_B shift is complicated by the fact that it consists of contributions due to chemical, configuration, and relaxation shifts.[104] These contributions are difficult to evaluate theoretically even for simple binary alloys.[104]

IV. CONCLUSIONS

The structure of the valence band of *i*-$Al_{65}Cu_{20}Ru_{15}$ consists of two main features with the maximum intensity at 1.3(1) and 3.8(1) eV below E_F. The first feature was shown to be due mainly to the Ru 4*d*-derived states, whereas the other was demonstrated to result from the states of the predominantly Cu 3*d* character. The Ru 4*d* and Cu 3*d* partial density of states were determined empirically from the measured valence bands. It was shown that the density of states of each of these two elements is distributed throughout the width of the band. The decrease of intensity as the energy approaches E_F was interpreted as indicative of the presence of the minimum of the DOS around E_F. It was indicated, however, that the Fermi cutoff also contributes to the observed intensity decrease. It was demonstrated that high-energy-resolution experiments probing the DOS below and above E_F are essential to unambiguously determine the possible presence of such a pseudogap in quasicrystals. The presently available spectroscopic data were obtained with insufficiently high-energy-resolution to convincingly demonstrate the presence of such a pseudogap. The spikiness of the density of states predicted by theory was not observed within the energy resolution of the experiment. It was shown that such a spikiness can be detected only by using spectroscopic techniques of the highest available energy resolution.

ACKNOWLEDGMENTS

This work was supported by the Natural Sciences and Engineering Research Council of Canada and a Grant-in-Aid for Scientific Research from the Ministry of Education, Science, and Culture of Japan. The research was carried out (in part) at the National Synchrotron Light Source, Brookhaven National Laboratory, which is supported by the U.S. Department of Energy, Division of Materials Sciences and Division of Chemical Sciences (DOE Contract No. DE-AC02-76CH00016). Two of us (Z.M.S. and G.W.Z.) are deeply indebted to Dr. M.-L. Shek for her help in conducting the PES experiments and to Professor T. Fujiwara for the DOS of the $Al_{80}Cu_{32}Fe_{16}$ approximant.

*Author to whom all correspondence should be addressed.

[1]D. Shechtman, I. Blech, D. Gratis, and J. W. Cahn, Phys. Rev. Lett. **53**, 1951 (1984).

[2]*Quasicrystals, The State of the Art,* edited by D. P. DiVincenzo and P. J. Steinhardt (World Scientific, Singapore, 1991).

[3]A. I. Goldman and M. Widom, Annu. Rev. Phys. Chem. **42**, 685 (1991); *Quasicrystals,* edited by T. Fujiwara and T. Ogawa (Springer-Verlag, Berlin, 1990).

[4]P. A. Bruhwiler, J. L. Wagner, B. D. Biggs, Y. Shen, K. M. Wong, S. E. Schnatterly, and S. J. Poon, Phys. Rev. B **37**, 6529 (1988).

[5]D. L. Ederer, R. Schaefer, K.-L. Tsang, C. H. Zhang, T. A. Caliicott, and E. T. Arakawa, Phys. Rev. B **37**, 8594 (1988).

[6]U. Mizutani, A. Kamiya, T. Matsuda, K. Kihishi, and S. Takeuchi, J. Phys. Condens. Matter **3**, 3711 (1991).

[7]S. J. Poon, Adv. Phys. **41**, 303 (1992), and references therein.

[8]A.-P. Tsai, A. Inoue, and T. Masumoto, Jpn. J. Appl. Phys. **26**, L1505 (1987); **27**, L1587 (1988).

[9]A.P. Tsai, A. Inoue, Y. Yokoyama, and T. Masumoto, Mater. Trans., Jpn. Inst. Met. **31**, 98 (1990); Philos. Mag. Lett. **61**, 9 (1990); A.-P. Tsai, Y. Yokoyama, A. Inoue, and T. Masumoto, Jpn. J. Appl. Phys. **29**, L1161 (1990).

[10]P. Lanco, C. Berger, F. Cyrot-Lackmann, and A. Sulpice, J. Non-Cryst. Solids **153-154**, 325 (1993); H. Akiyama, T. Hashimoto, T. Shibuya, K. Edagawa, and S. Takeuchi, J. Phys. Soc. Jpn. **62**, 639 (1993); S. Takeuchi, H. Akiyama, N. Naito, T. Shibuya, K. Edagawa, and K. Kimura, J. Non-Cryst. Solids **153-154**, 353 (1993).

[11]F. S. Pierce, S. J. Poon, and Q. Guo, Science **261**, 737 (1993).

[12]H. Akiyama, Y. Honda, T. Hashimoto, K. Edagawa, and S. Takeuchi, Jpn. J. Appl. Phys. **32**, L1003 (1993); C. Berger, T. Grenet, P. Lindqvist, P. Lanco, J. C. Grieco, G. Fourcaudot, and F. Cyrot-Lackmann, Solid State Commun. **87**, 977 (1993).

[13]T. Klein, C. Berger, D. Mayou, and F. Cyrot-Lackmann, Phys. Rev. Lett. **66**, 2907 (1991).

[14]S. Kimura and S. Takeuchi, in *Quasicrystals, The State of the Art* (Ref. 2), p. 313, and references therein.

[15]Z. M. Stadnik, G. Stroink, H. Ma, and G. Williams, Phys. Rev. B **39**, 9797 (1989), and references therein.

[16]S. Matsuo, T. Ishimasa, H. Nakano, and Y. Fukano, J. Phys. F **18**, L175 (1988).

[17]S. Matsuo, H. Nakano, T. Ishimasa, and Y. Fukano, J. Phys. Condens. Matter **1**, 6893 (1989).

[18]T. Klein, A. Gozlan, C. Berger, F. Cyrot-Lackmann, Y. Calvayrac, A. Quivy, and G. Fillion, Physica B **165-166**, 283 (1990).

[19]P. Lanco, T. Klein, C. Berger, F. Cyrot-Lackmann, G. Fourcaudot, and A. Sulpice, Europhys. Lett. **18**, 227 (1992).

[20]C. L. Chien and M. Lu, Phys. Rev. B **45**, 12 793 (1992).

[21]A. P. Smith and N. W. Ashcroft, Phys. Rev. Lett. **59**, 1365 (1987); J. Friedel and F. Dénoyer, C. R. Acad. Sci. (Paris) **305**, 171 (1987); V. G. Vaks, V. V. Kamyshenko, and G. D. Samolyuk, Phys. Lett. A **132**, 131 (1988); J. Friedel, Helv. Phys. Acta **61**, 538 (1988); Philos. Mag. B **65**, 1125 (1992); M. A. Fradkin, J. Phys. Condens. Matter **4**, 10 497 (1992).

[22]T. Fujiwara, Phys. Rev. B **40**, 942 (1989); J. Non-Cryst. Solids **117-118**, 844 (1990); T. Fujiwara and H. Tsunetsugu, in *Quasicrystals, The State of the Art* (Ref. 2), p. 343; T. Fujiwara and T. Yokokawa, Phys. Rev. Lett. **66**, 333 (1991). T. Fujiwara, J. Non-Cryst. Solids **156-158**, 865 (1993); T. Fujiwara, S. Yamamoto, and G. Trambly de Laissardière, Phys. Rev. Lett. **71**, 4166 (1993).

[23]J. Hafner and M. Krajčí, Phys. Rev. Lett. **68**, 2321 (1992); Europhys. Lett. **17**, 145 (1992); J. Non-Cryst. Solids **150**, 337 (1992).

[24]J. Hafner and M. Krajčí, Phys. Rev. B **47**, 11 795 (1993).

[25]A. E. Carlsson, Phys. Rev. B **47**, 2515 (1993); J. Non-Cryst. Solids **153-154**, 386 (1993).

[26]F. Hippert, L. Kandel, Y. Calvayrac, and B. Dubost, Phys. Rev. Lett. **69**, 2086 (1992).
[27]J. C. Phillips and K. M. Rabe, Phys. Rev. Lett. **66**, 923 (1991); J. C. Phillips, Solid State Commun. **83**, 379 (1992); Phys. Rev. B **47**, 2522 (1993); **47**, 7747 (1993).
[28]D. Mayou, C. Berger, F. Cyrot-Lackmann, T. Klein, and P. Lanco, Phys. Rev. Lett. **70**, 3915 (1993).
[29]H. Tsunetsugu, T. Fujiwara, K. Ueda, and T. Tokihiro, Phys. Rev. B **43**, 8879 (1991); B. Passaro, C. Sire, and V. G. Benza, *ibid.* **46**, 13 751 (1992).
[30]M. A. Chernikov, A. Bernasconi, C. Beeli, and H. R. Ott, Europhys. Lett. **21**, 767 (1993), and references therein.
[31]N. Koshikawa, S. Sakamoto, K. Edagawa, and S. Takeuchi, Jpn. J. Appl. Phys. **31**, L966 (1992); N. Koshikawa, K. Edagawa, and S. Takeuchi, Mater. Trans. Jpn. Inst. Met. **34**, 188 (1993).
[32]A. Niikura, A. P. Tsai, A. Inoue, and T. Masumoto, Philos. Mag. Lett. **69**, 351 (1994); A. P. Tsai, A. Niikura, A. Inoue, T. Masumaoto, Y. Nishida, and M. Tanaka, *ibid.* **70**, 169 (1994).
[33]Ch. Janot and J. M. Dubois, J. Phys. F **18**, 2303 (1988).
[34]A. Shastri, F. Borsa, A. I. Goldman, J. E. Shield, and D. R. Torgeson, J. Non-Cryst. Solids **153-154**, 347 (1993).
[35]A. Shastri, F. Borsa, D. R. Torgeson, and A. I. Goldman, Phys. Rev. B **50**, 4224 (1994).
[36]N. Vernier, G. Bellessa, B. Perrin, A. Zarembovitch, and M. De Boissieu, Europhys. Lett. **22**, 187 (1993).
[37]A. Traverse, L. Dumoulin, and E. Belin, in *Quasicrystalline Materials,* edited by Ch. Janot and J. M. Dubois (World Scientific, Singapore, 1988), p. 399.
[38]E. Belin and A. Traverse, J. Phys. Condens. Matter **3**, 2157 (1991).
[39]M. Mori, S. Matsuo, T. Ishimasa, T. Matsuura, K. Kamiya, H. Inokuchi, and T. Matsukawa, J. Phys. Condens. Matter **3**, 767 (1991).
[40]H. Matsubara, S. Ogawa, T. Kinoshita, K. Kishi, S. Takeuchi, K. Kimura, and S. Suga, Jpn. J. Appl. Phys. A **30**, L389 (1991).
[41]M. Mori, K. Kamiya, S. Matsuo, T. Ishimasa, H. Nakano, H. Fujimoto, and H. Inokuchi, J. Phys. Condens. Matter **4**, L157 (1992).
[42]E. Belin, J. Kojnok, A. Sadoc, A. Traverse, M. Harmelin, C. Berger, and J.-M. Dubois, J. Phys. Condens. Matter **4**, 1057 (1992).
[43]E. Belin, Z. Dankhazi, A. Sadoc, Y. Calvayrac, T. Klein, and J.-M. Dubois, J. Phys. Condens. Matter **4**, 4459 (1992).
[44]E. Belin, in *Physics and Chemistry of Finite Systems,* edited by P. Jena, S. N. Khanna, and B. K. Rao (Kluwer, Amsterdam, 1992), Vol. II, p. 829.
[45]E. Belin and Z. Danhkázi, J. Non-Cryst. Solids **153-154**, 298 (1993).
[46]A. Sadoc, E. Belin, Z. Dankhazi, and A. M. Flank, J. Non-Cryst. Solids **153-154**, 338 (1993).
[47]E. Belin, Z. Dankhazi, and A. Sadoc, J. Non-Cryst. Solids **156-158**, 896 (1993).
[48]Z. M. Stadnik and G. Stroink, Phys. Rev. B **47**, 100 (1993), and references therein; J. Non-Cryst. Solids **156-158**, 891 (1993).
[49]E. Belin and D. Mayou, Phys. Scr. **T49**, 356 (1993).
[50]U. Mizutani, T. Matsuda, Y. Itoh, K. Tanaka, H. Domae, T. Mizuno, S. Murasaki, Y. Miyoshi, K. Hashimoto, and Y. Yamada, J. Non-Cryst. Solids **156-158**, 882 (1993).
[51]G. W. Zhang, Z. M. Stadnik, A.-P. Tsai, and A. Inoue, Phys. Lett. A **186**, 345 (1994); Phys. Rev. B **50**, 6696 (1994), and references therein.
[52]P. Häussler, Phys. Rep. **222**, 65 (1992), and references therein.
[53]M. E. McHenry, M. E. Eberhart, R. C. O'Handley, and K. H. Johnson, Phys. Rev. Lett. **56**, 81 (1986); R. C. O'Handley, R. A. Dunlap, and M. E. McHenry, in *Handbook of Magnetic Materials,* edited by K. H. J. Buschow (Elsevier, Amsterdam, 1991), Vol. 6, p. 453.
[54]V. De Coulon, F. A. Reuse, and S. N. Khanna, Phys. Rev. B **48**, 814 (1993); F. Liu, S. N. Khanna, L. Magaud, P. Jena, V. De Coulon, X-G. He, and F. Cyrot-Lackman, *ibid.* **48**, 1295 (1993).
[55]C. A. Guryan, A. I. Goldman, P. W. Stephens, K. Hiraga, A. P. Tsai, A. Inoue, and T. Masumoto, Phys. Rev. Lett. **62**, 2409 (1989).
[56]A.-P. Tsai, A. Inoue, and T. Masumoto, Mater. Trans. Jpn. Inst. Met. **30**, 666 (1989).
[57]K. Hiraga, M. Hirabayashi, A. P. Tsai, A. Inoue, and T. Masumoto, Philos. Mag. Lett. **60**, 201 (1989).
[58]E. Matsubara and Y. Waseda, in *Quasicrystals,* edited by K. H. Kuo and T. Ninomiya (World Scientific, Singapore, 1991), p. 96.
[59]R. Hu, T. Egami, A.-P. Tsai, and A. Inoue, T. Masumoto, J. C. Holtzer, and K. Kelton, in *Physics and Chemistry of Finite Systems* (Ref. 44), Vol. I, p. 39.
[60]J. E. Shield, C. Hoppe, R. W. McCallum, A. I. Goldman, K. F. Kelton, and P. C. Gibbons, Phys. Rev. B **45**, 2063 (1992); J. E. Shield, L. S. Chumbley, R. W. McCallum, and A. I. Goldman, J. Mater. Res. **8**, 44 (1993).
[61]K. Araki, A. Waseda, K. Kimura, and H. Ino, Philos. Mag. Lett. **67**, 351 (1993).
[62]A. Sadoc, C. Berger, and Y. Calvayrac, Philos. Mag. B **68**, 475 (1993).
[63]K. Hiraga, K. H. Lee, M. Hirabayashi, A.-P. Tsai, A. Inoue, and T. Masumoto, Jpn. J. Appl. Phys. **28**, L1624 (1989).
[64]M. Cornier-Quiquandon, A. Quivy, S. Lefebvre, E. Elkaim, G. Heger, A. Katz, and D. Gratias, Phys. Rev. B **44**, 2071 (1991).
[65]M. Boudard, M. De Boissieu, C. Janot, G. Heger, C. Beeli, H.-U. Nissen, H. Vincent, R. Ibberson, M. Audier, and J. M. Dubois, J. Phys. Condens. Matter **4**, 10 149 (1992).
[66]B. D. Biggs, S. J. Poon, and N. R. Munirathnam, Phys. Rev. Lett. **65**, 2700 (1990); B. D. Biggs, S. J. Poon, and F. S. Pierce, in *Physics and Chemistry of Finite Systems* (Ref. 44), Vol. II, p. 819.
[67]U. Mizutani, Y. Sakabe, T. Shibuya, K. Kishi, K. Kimura, and S. Takeuchi, J. Phys. Condens. Matter **2**, 6169 (1990).
[68]K. Kimura, K. Kishi, T. Hashimoto, S. Takeuchi, and T. Shibuya, Mater. Sci. Eng. A **133**, 95 (1991); K. Kimura, K. Kishi, T. Hashimoto, and S. Takeuchi, in *Quasicrystals* (Ref. 58), p. 233.
[69]F. S. Pierce, P. A. Bancel, B. D. Biggs, Q. Guo, and S. J. Poon, Phys. Rev. B **47**, 5670 (1993).
[70]F. S. Pierce, S. J. Poon, and B. D. Biggs, Phys. Rev. Lett. **70**, 3919 (1993).
[71]S. J. Poon, Mater. Sci. Eng. B **19**, 72 (1993); J. Non-Cryst. Solids **153-154**, 334 (1993).
[72]N. F. Mott, *Conduction in Non-Crystalline Materials* (Clarendon, Oxford, 1993).
[73]T. Shinohara, A. P. Tsai, T. Sato, and T. Masumoto, J. Mater. Res. **7**, 1970 (1992).
[74]E. A. Hill, T. C. Chang, Y. Wu, S. J. Poon, F. S. Pierce, and Z. M. Stadnik, Phys. Rev. B **49**, 8615 (1994).
[75]W. Wong-Ng and C. R. Hubbard, Powder Diffr. **2**, 242 (1987).
[76]D. L. Bish and S. J. Chipera, Powder Diffr. **4**, 137 (1989).
[77]R. Jenkins and W. N. Schreiner, Powder Diffr. **4**, 74 (1989).
[78]W. N. Schreiner and R. Jenkins, Adv. X-ray Anal. **26**, 141

(1983).
[79]J. W. Cahn, D. Shechtman, and D. Gratias, J. Mater. Res. **1**, 13 (1986).
[80]V. Elser, Acta Cryst. A **42**, 36 (1986).
[81]P. A. Bancel, P. A. Heiney, P. W. Stephens, A. I. Goldman, and P. M. Horn, Phys. Rev. Lett. **54**, 2422 (1985).
[82]J. Devaud-Rzepski, A. Quivy, Y. Calvayrac, M. Cornier-Quiquandon, and D. Gratias, Philos. Mag. B **60**, 855 (1989).
[83]J. C. Helmer and N. H. Weichert, Appl. Phys. Lett. **13**, 266 (1968).
[84]D. A. Shirley, Phys. Rev. B **5**, 4709 (1972).
[85]J. J. Yeh, *Atomic Calculation of Photoionization Cross-Sections and Asymmetry Parameters* (Gordon and Breach, New York, 1993).
[86]L. C. Davis, J. Appl. Phys. **59**, R25 (1986), and references therein.
[87]C. Kunz, in *Photoemission in Solids II,* edited by L. Ley and M. Cardona (Springer-Verlag, Berlin, 1979), p. 299.
[88]G. Rossi, I. Lindau, L. Braicovich, and I. Abbati, Phys. Rev. B **28**, 3031 (1983), and references therein.
[89]D. E. Eastman and W. D. Grobman, Phys. Rev. Lett. **28**, 1327 (1972); J. Freeouf, M. Erbudak, and D. E. Eastman, Solid State Commun. **13**, 771 (1973); P. J. Feibelman and D. E. Eastman, Phys. Rev. B **10**, 4932 (1974).
[90]H. Wright, P. Weightman, P. T. Andrews, W. Folkerts, C. F. J. Flipse, G. Sawatzky, D. Norman, and H. Padmore, Phys. Rev. B **35**, 519 (1987).
[91]W. Folkerts, D. Van Der Marel, C. Haas, G. A. Sawatzky, D. Norman, H. Padmore, H. Wright, and P. Weightman, J. Phys. F **17**, 657 (1987).
[92]J. W. Allen, S. J. Oh, O. Gunnarsson, K. Schönhammer, M. B. Maple, M. S. Torikachvili, and I. Lindau, Adv. Phys. **35**, 275 (1986), and references therein; K. Soda, T. Mori, M. Taniguchi, S. Asaoka, K. Naito, Y. Ōnuki, T. Komatsubara, T. Miyahara, S. Sato, and T. Ishii, J. Phys. Soc. Jpn. **55**, 1709 (1986); Z.-X. Shen, P. A. P. Lindberg, B. O. Wells, D. S. Dessau, A. Borg, I. Lindau, W. E. Spicer, W. P. Ellis, G. H. Kwei, K. C. Ott, J.-S. Kang, and J. W. Allen, Phys. Rev. B **40**, 6912 (1989); R. Weidmann, H.-E. Gumlich, M. Kupsch, H.-U. Middelmann, and U. Becker, *ibid.* **45**, 1172 (1992); S. Nohara, H. Namatame, A. Fujimori, and T. Takabatake, *ibid.* **47**, 1754 (1993); Y. Ueda, M. Taniguchi, T. Mizokawa, A. Fujimori, I. Souma, and Y. Oka, *ibid.* **49**, 2167 (1994).
[93]Y. Baer and G. Busch, Phys. Rev. Lett. **30**, 280 (1973).
[94]G. Trambly de Laissardière and T. Fujiwara, Phys. Rev. B **50**, 5999 (1994).
[95]E. Cockayne, R. Phillips, X. B. Kan, S. C. Moss, J. L. Robertson, T. Ishimasa, and M. Mori, J. Non-Cryst. Solids **153-154**, 140 (1993).
[96]H. Höchst, P.Steiner, G. Reiter, and S. Hüfner, Z. Phys. B **42**, 199 (1981).
[97]F. Patthey, B. Delley, W.-D. Schneider, and Y. Baer, Phys. Rev. Lett. **55**, 1518 (1985); E. Weschke, C. Laubschat, T. Simmons, M. Domke, O. Strebel, and G. Kaindl, Phys. Rev. B **44**, 8304 (1991); Y. Hwu, L. Lozzi, S. La Rosa, M. Onellion, P. Almeras, F. Gozzo, F. Lévy, H. Berger, and G. Margaritondo, *ibid.* **45**, 5438 (1992).
[98]J.-M. Imer, F. Patthey, B. Dardel, W.-D. Schneider, Y. Baer, Y. Petroff, and A. Zettl, Phys. Rev. Lett. **62**, 336 (1989); C. G. Olson, R. Liu, A.-B. Yang, D. W. Lynch, A. J. Arko, R. S. List, B. W. Veal, Y. C. Chang, P. Z. Jiang, and A. P. Paulikas, Science **245**, 731 (1989); Z.-X. Shen, D. S. Dessau, B. O. Wells, D. M. King, W. E. Spicer, A. J. Arko, D. Marshall, L. W. Lombardo, A. Kapitulnik, P. Dickinson, S. Doniach, J. DiCarlo, A. G. Loeser, and C. H. Park, Phys. Rev. Lett. **70**, 1553 (1993).
[99]D. Dardel, M. Grioni, D. Malterre, P. Weibel, Y. Baer, and F. Lévy, J. Phys. Condens. Matter **5**, 6111 (1993), and references therein.
[100]T. Takahashi, Comments Condens. Matter Phys. **16**, 113 (1992), and references therein.
[101]S. Doniach and M. Šunjić, J. Phys. C **3**, 285 (1970).
[102]Y. Baer, G. Busch, and P. Cohn, Rev. Sci. Instrum. **46**, 466 (1975); S. A. Flodstrom, R. Z. Bachrach, R. S. Bauer, and S. B. Hagström, Phys. Rev. Lett. **37**, 1282 (1976).
[103]F. U. Hillebrecht, J. C. Fuggle, P. A. Bennett, Z. Zołnierek, and Ch. Freiburg, Phys. Rev. B **27**, 2179 (1983).
[104]Z. M. Stadnik and G. Stronik, J. Non-Cryst. Solids **99**, 233 (1988), and references therein.